Loss of KIF13B causes time-dependent changes in ciliary polycystin-2 levels and extracellular vesicle release

Csenge K. Rezi[1, *], Alina Frei[2, *], Fabiola Campestre[1], Christina R. Berggreen[1], Julie Laplace[1, 4], Aurelien Sicot[1, 5], Geyi Li[1], Søren L. Johansen[1], Julie K. T. Sørensen[1, 6], Martin W. Berchtold[1], Mohamed Chamlali[1], Søren T. Christensen[1], Karsten Boldt[3], Zeinab Anvarian[1, #], Helen L. May-Simera[2, #], Lotte B. Pedersen[1, #]

[1]Department of Biology, University of Copenhagen, Universitetsparken 13, DK-2100 Copenhagen Ø, Denmark

[2]Institute of Molecular Physiology, Johannes Gutenberg-University, Mainz, Germany

[3]Medical Bioanalytics, Institute for Ophthalmic Research, Eberhard-Karls University, Tübingen, Germany

[4]Present address: École Normale Supérieure Paris-Saclay, Department of Biology, 4 Avenue des Sciences, 91190 Gif-sur-Yvette, France

[5]Present address: Sim&Cure, 95 rue Pierre Flourens, Bâtiment H, 34000 Montpellier, France

[6]Present address: AJ Vaccines A/S, Artillerivej 5, DK-2300 Copenhagen S, Denmark

*These authors contributed equally

[#]Joint corresponding authors

Further information and requests for resources and reagents should be directed the lead contact Lotte B. Pedersen (lbpedersen@bio.ku.dk)

Key words: primary cilia, polycystin-2, kinesin-3, KIF13B, extracellular vesicle, HRS, TSG101, ITCH, ALIX, ZDHHC5, polycystic kidney disease, ADPKD

Abstract

The polycystic kidney disease gene product polycystin-2 (PC2) localizes to and is released from primary cilia in extracellular vesicles (EVs). We report that KIF13B regulates ciliary EV release and PC2 levels in kidney epithelial cells in a time-dependent manner and show that KIF13B itself is released from the ciliary tip. In early stages of ciliation, *Kif13b*$^{-/-}$ cells displayed excessive ciliary accumulation of PC2 and initially released fewer small EVs than control cells. Over time, ciliated *Kif13b*$^{-/-}$ cells increased their small EV release rate to control levels, however proteomic analysis identified >50 proteins depleted from mutant EV samples. These included the ubiquitin E3 ligase ITCH and palmitoyl transferase ZDHHC5, which localized to primary cilia. Mature *Kif13b*$^{-/-}$ cilia exhibited aberrant membrane bulges and decreased PC2 and ALIX, an ITCH substrate that negatively regulated ciliary PC2 levels. Our work provides new insight into the mechanisms of ciliary EV release, which is important for regulating ciliary membrane homeostasis and signalling function.

Introduction

Primary cilia are antenna-like sensory organelles that protrude from the surface of many vertebrate cell types, including polarized kidney epithelial cells, and play important roles in coordinating a range of developmental and homeostatic signaling pathways that regulate cell behavior, cell cycle progression and differentiation (Anvarian et al., 2019, Mill et al., 2023). Mutations in genes that regulate cilia assembly, maintenance or function are causative of pleiotropic diseases called ciliopathies, which include several diseases with renal phenotypes, e.g. nephronophthisis (NPHP), Bardet-Biedl Syndrome (BBS) and polycystic kidney disease (PKD) (Reiter and Leroux, 2017, Mill et al., 2023).

The ciliary membrane, which ensheathes the microtubule-based axoneme, is enriched for specific proteins (e.g. receptors and ion channels) and lipids (e.g. phosphoinositides) that function in various signaling pathways (Nachury and Mick, 2019, Nguyen et al., 2022). For example, in kidney epithelial cells the transmembrane proteins polycystin-1 (PC1) and polycystin-2 (PC2), which are encoded by the autosomal dominant (AD) PKD genes *PKD1* and *PKD2*, respectively (Hughes et al., 1995, Mochizuki et al., 1996), are highly concentrated in primary cilia (Yoder et al., 2002, Pazour et al., 2002). Here they form a calcium-permeable nonselective cation channel complex required for maintaining normal renal tubular structure and function. Mutations in *PKD1*, *PKD2* or other genes that impair ciliary localization of PC1 or PC2 are associated with ADPKD, indicating that appropriate regulation of ciliary targeting and homeostasis of the PC1-PC2 complex is critical for kidney development, homeostasis and function (Ma et al., 2017, Hu and Harris, 2020, Luo et al., 2023).

In polarized kidney epithelial cells, targeting of transmembrane proteins from their site of synthesis in the ER/Golgi to the primary cilium is complex, and the specific vesicular trafficking route employed can vary from protein to protein (Monis et al., 2017, Zhao et al., 2023). For example, post-Golgi vesicles carrying PC2 are thought to be transported via recycling endosomes and/or the plasma membrane prior to reaching the base of the primary cilium where the vesicles dock at the transition fibers; PC2 then crosses the transition zone and is imported into the cilium (Monis et al., 2017, Walker et al., 2019, Hu and Harris, 2020). Multiple factors that regulate specific stages of ciliary PC2 trafficking have been identified (Hu and Harris, 2020), including IFT20 (Follit et al., 2006, Follit et al., 2008), SDCCAG3 (Yu et al., 2016), BLOC-1 (Monis et al., 2017) and exocyst complexes (Fogelgren et al.,

2011), as well as DLG1 (Rezi et al., 2023) and the small GTPases RAB8 (Hoffmeister et al., 2011) and RAB11 (Monis et al., 2017). Following import into the cilium, additional mechanisms are employed to down-regulate ciliary PC2 levels and ensure organelle homeostasis, including endocytic retrieval and release of PC2-containing extracellular vesicles (EVs) (Hu and Harris, 2020).

Extracellular vesicles are released by many cell types and mediate intercellular transport of different macromolecules to regulate various physiological and pathological processes (Dixson et al., 2023). Both primary and motile cilia are known to release EVs, which may serve to regulate ciliary membrane homeostasis and intercellular signaling (Wood and Rosenbaum, 2015, Akella and Barr, 2021, Volz et al., 2021, Ojeda Naharros and Nachury, 2022). In general, two major subtypes of EVs have been categorized based on their origin: exosomes, which are small (ca. 50-150 nm in diameter) and derived from the multivesicular body (MVB), and ectosomes, which vary in size from ca. 100 nm to several micrometers in diameter and arise from outward protrusions of the plasma membrane that are subsequently excised and released into the environment (Dixson et al., 2023). It is thought that EVs derived from cilia are ectosomes, generated by outward budding of the ciliary membrane (Wood and Rosenbaum, 2015), which may range in size and content depending on whether they are released from the ciliary tip or base (Clupper et al., 2022). Hereafter, exosomes and small ectosomes are designated small EVs, and larger ectosomes are designated large EVs.

The relationship between ciliary PC1/PC2 homeostasis and EV release has been particularly well studied in ciliated male sensory neurons of *Caenorhabditis elegans*. In these cilia, homologs of mammalian PC1 (LOV-1) and PC2 (PKD-2) associate with the ESCRT-0 proteins HRS and STAM, which function on early endosomes to direct the LOV-1-PKD-2 complex for lysosomal degradation hence promoting its removal from cilia (Hu et al., 2007). This pathway may also involve caveolin-1 (CAV1), which together with endosome maturation factors Rabenosyn-5 and VPS45 promotes endocytic retrieval of PKD-2 at the periciliary membrane compartment (Scheidel et al., 2018). The cilia also release PKD-2-containing EVs to regulate male-mating behavior by a mechanism involving the kinesin-3 motor protein KLP-6; in *klp-6* mutant animals such EVs are not released into the environment causing excessive shedding of EVs into the glial lumen surrounding the ciliary base (Wang et al., 2014). The release of polycystin-containing EVs from cilia is evolutionarily conserved as polycystin homologs were detected in cilia-derived EVs purified from the green alga

Chlamydomonas reinhardtii (Wood et al., 2013, Long et al., 2016), in EVs isolated from human urine (Hogan et al., 2009) as well as the mouse embryonic node (Tanaka et al., 2023). However, the mechanisms underlying ciliary polycystin homeostasis and EV release in vertebrates remain incompletely understood.

We previously showed that a mammalian homolog of *C. elegans* KLP-6, the kinesin-3 motor protein KIF13B, localizes to primary cilia of hTERT-immortalized human retinal pigment epithelial (RPE1) cells where it mediates formation of a CAV1-enriched membrane domain at the transition zone, thereby regulating Sonic hedgehog signaling (Schou et al., 2017). Furthermore, we found that KIF13B undergoes transient and burst-like movement within primary cilia of RPE1 cells and is occasionally released from cilia in EV-like particles (Juhl et al., 2023). Here we demonstrate a role for KIF13B in regulating ciliary PC2 levels and EV biogenesis in cultured mouse cortical collecting duct (mCCD) cells (Montesano et al., 2009) and show that loss of KIF13B affects these processes in a time-dependent manner. Specifically, we found that *Kif13b*$^{-/-}$ mCCD cells with newly assembled cilia displayed excessive ciliary accumulation of PC2 and released fewer small EVs compared to control cells. The mutant-derived small EVs were also compositionally different, containing reduced levels of HRS and Thrombospondin-1 (THBS1). However, upon prolonged serum-starvation to induce cilia maturation, the *Kif13b*$^{-/-}$ cells gradually modulated their release and content of small and large EVs, which was accompanied by reduced ciliary levels of PC2 and the ESCRT accessory protein ALIX, whose depletion also affected ciliary PC2 homeostasis. Consistent with a role for KIF13B in promoting EV release from cilia, live cell imaging analysis demonstrated burst-like movement of KIF13B within primary cilia of mCCD cells and KIF13B was itself released in EVs. Our results therefore identify a new role for KIF13B in regulating ciliary PC2 homeostasis and EV release in kidney epithelial cells. Furthermore, our data indicates that these cells may alter EV biogenesis and release over time to compensate for an initial imbalance in ciliary membrane protein homeostasis.

Results

Loss of KIF13B causes time-dependent changes in ciliary PC2 levels

In *C. elegans*, kinesin-3 motor KLP-6 regulates ciliary localization and EV shedding of PKD-2 (Peden and Barr, 2005, Wang et al., 2014, Wang et al., 2021). To test if KIF13B similarly regulates ciliary PC2 localization and EV shedding, we knocked out *Kif13b* in mCCD cells and confirmed the absence of KIF13B in *Kif13b*$^{-/-}$ cells by western blotting (Figure 1a). Consistent with previous work (Montesano et al., 2009, Rezi et al., 2023) mCCD cells formed primary cilia upon serum starvation for 24 or 72 h, and loss of KIF13B did not affect ciliation frequency or ciliary length under these conditions (Figure S1a-c; see also Figure 5a). Total cellular levels of PC2 in *Kif13b*$^{-/-}$ cells were similar to those of wild type (WT) cells, both for cells grown in the presence of serum (+FBS) or depleted for serum for 24, 48, or 72 h (Figure 1a, b; Figure S1d). We then analyzed the ciliary localization of PC2 in WT and *Kif13b*$^{-/-}$ cells by immunofluorescence microscopy (IFM). Using a previously described anti-PC2 antibody (He et al., 2018) to stain for PC2 in 24 h serum-starved cells, we found significant accumulation of PC2 within cilia of *Kif13b*$^{-/-}$ cells, as compared to WT cells (Figure 1c, d). Stable expression of mCherry-KIF13B in the *Kif13b*$^{-/-}$ cells (Figure S1e, f) rescued this phenotype (Figure 1c, d), and similar results were obtained using an alternative antibody against PC2 (Figure 1e, f). Conversely, in 72 h serum-starved cells, ciliary PC2 levels in *Kif13b*$^{-/-}$ mutant cells were significantly lower than for WT cells, and this phenotype was rescued by stable expression of mCherry-KIF13B (Figure 1e, f). Thus, KIF13B regulates ciliary PC2 levels in a time-dependent manner.

KIF13B regulates release and composition of small EVs

Next, we investigated if KIF13B might regulate ciliary PC2 homeostasis by modulating its release in EVs. First, we performed live cell imaging of mCCD cells stably expressing mNeonGreen-KIF13B in the *Kif13b*$^{-/-}$ background (Figure S1f) and subjected the cells to 24-72 h of serum starvation. In cells serum-starved for 24-48 h, we found that mNeonGreen-KIF13B transiently accumulates and moves bidirectionally within 21% of cilia analysed (n=72; Movie 1), reminiscent of our previous observations in ciliated hTERT-RPE1 cells transiently expressing eGFP-KIF13B (Juhl et al., 2023). Similar observations were made for cells serum-starved for 72, where mNeonGreen-KIF13B transiently accumulated and moved within 33% of cilia analysed (n=30). In addition, under these conditions mNeonGreen-

KIF13B appeared to be released from the ciliary tip (Figure 2; Movie 2), as seen previously in ciliated hTERT-RPE1 cells transiently expressing eGFP-KIF13B (Juhl et al., 2023).

Next, we collected spent medium from WT and *Kif13b*$^{-/-}$ mCCD cell cultures following 24, 48 or 72 h of serum starvation and used two different approaches to purify small and/or large EVs for downstream analyses. First, using a previously published differential centrifugation protocol (Volz et al., 2021) we purified small EVs from spent medium of 24, 48 and 72 h serum-starved WT and *Kif13b*$^{-/-}$cultures, respectively (Figure 3a). Successful purification of small EVs was confirmed by transmission electron microscopy (TEM), which revealed the characteristic presence of spherical biconcave structures 100-200 nm in size (Figure 3b), and by western blot analysis using antibodies specific for common small EV marker proteins (Figure S2a). Nanoparticle tracking analysis (NTA) showed a significant decrease in the number of small EVs released from 24 h serum-deprived *Kif13b*$^{-/-}$ cultures compared to WT controls (Figure 3c). Intriguingly, prolonged serum-deprived conditions (72 h in total) caused a significant increase in the relative rate of small EVs release in the *Kif13b*$^{-/-}$ cells bringing the rate of release comparable to WT levels, which compensated the difference at baseline release after 24 h (Figure 3c, d), suggesting an adaptive mechanism in small EV release in the *Kif13b*$^{-/-}$ cells over time. Treatment of the 24 h serum-starved cultures with GW4869, an inhibitor of ceramide-dependent intraluminal vesicle budding into MVBs (Dixson et al., 2023), led to an overall reduction in small EV numbers for both cell lines, as expected, suggesting that a significant proportion of small EVs are MVB-derived (Figure 3e, f). However, the inhibitory effect of GW4869 treatment on the number of small EVs released from WT cultures was much more pronounced compared to that of *Kif13b*$^{-/-}$ cultures (Figure 3e, f), suggesting that the *Kif13b*$^{-/-}$ cells may already be impaired in small EV release via the ceramide-dependent MVB pathway.

To determine if loss of KIF13B affects the protein content of small EVs, we analyzed small EV samples from 24 and 72 h serum-starved WT and *Kif13b*$^{-/-}$ cultures by mass spectrometry (MS) using an established protocol (Volz et al., 2021). We found that for the 24 h small EV samples only two proteins, THBS1 and HRS/HGS (hereafter: HRS), were significantly depleted from the *Kif13b*$^{-/-}$ samples compared to WT (Figure 4a; Table S1). For the 72 h samples 52 proteins were significantly altered in the *Kif13b*$^{-/-}$ sample compared to WT, with the majority being depleted from the mutant-derived EVs (Figure 4b; Table S2). Gene Ontology (GO) term enrichment analysis of the latter proteins, focusing on the two GO categories Cellular Component and Molecular Function, identified focal adhesion,

extracellular exosome, GTP binding and RNA binding as the most highly enriched GO terms in this dataset (Figure 4c, d). Specific proteins depleted from the 72 h mutant EV samples included the clathrin adaptor AP2A1; TTC8, a BBS protein (Ansley et al., 2003) and known component of the BBSome that functions as retrograde IFT membrane protein cargo adapter (Nachury et al., 2007, Nachury and Mick, 2019); the acid ceramidase ASAH2; the deubiquitinase STAMBP, which regulates cell surface receptor trafficking at ESCRT-0 positive endosomes by directly binding to the HRS-STAM complex and regulating its ubiquitination status (Wright et al., 2011); the ubiquitin E3 ligase ITCH that binds and ubiquitylates several proteins including ALIX, HRS, STAM and SCAMP3 (O'Connor et al., 2015); and the palmitoyltransferase ZDHHC5 (Figure 4b; Table S2). PC1 and PC2 were also detected in our small EV proteomes of 72 h serum-starved WT and *Kif13b*$^{-/-}$ cultures but were unchanged in relative abundance in the mutant EVs compared to WT under these conditions. We did not detect PC1 nor PC2 in small EVs from 24 h serum-starved cultures (Table S1). Interestingly, we noted that HRS, as well as eleven of the proteins that were significantly depleted in abundance in the 72 h *Kif13b*$^{-/-}$ EV samples compared to WT samples (Figure 4e), have also been reported to be enriched in small EVs purified from *Bbs4* and/or *Bbs6* mutant kidney epithelial cells (Volz et al., 2021). This suggests that KIF13B and the BBSome act in opposite ways to control release of these proteins in small EVs. Collectively, the NTA and MS analyses of our small EV samples indicate that loss of KIF13B in mCCD cells modulates the release frequency and protein content of small EVs in a time-dependent manner, reflecting alterations in specific endo-lysosomal pathways including the ceramide-dependent and HRS-STAM pathways.

Since our analyses of small EVs, purified via ultracentrifugation, did not reveal any impact of KIF13B loss on the EV-mediated release of PC1/PC2 (Table S2), we tested whether KIF13B modulates release of polycystins in large EVs. We used an alternative approach to purify both large and small EVs from 72 h serum-starved WT and *Kif13b*$^{-/-}$ spent medium by centrifugation (large EVs) and lectin-mediated precipitation (small EVs) (Samsonov et al., 2016) (Figure S2b). Western blotting for EV markers (ARF6, TSG101, ALIX) confirmed the presence of these markers in our EV samples, while absence of the cis-Golgi marker GM130 ruled out cellular contamination (Figure S2c). Ciliary proteins like ARL13B, acetylated α-tubulin and PC2 were detected in both large and small EV fractions, and KIF13B itself was abundantly present in large EVs (Figure S2c, d), in line with our live cell imaging analysis (Figure 2; Movie 2) and evidence from *C. elegans* identifying KLP-6 in neuronal ciliary EVs

(Nikonorova et al., 2022). Moreover, for the *Kif13b*$^{-/-}$ cells we observed a significant shift in distribution of PC2 and TSG101 from large to small EV fractions, as compared to WT cells (Figure S2c, d), indicating that in 72 h serum-starved cells, KIF13B promotes the release of PC2 and TSG101 in large EVs and that loss of KIF13B causes these proteins to be released via small EVs instead. We similarly attempted to purify large and small EVs from 24 h serum-starved cultures, but the results were inconclusive due to poor yields. Therefore, it remains to be clarified if KIF13B also promotes release of PC2 in large EVs from 24 h serum-starved cells.

Increased ciliary membrane bulging in cells lacking KIF13B

To further investigate if KIF13B affects release of EVs directly from the ciliary membrane, we analyzed ciliary morphology of 72 h serum-deprived WT and *Kif13b*$^{-/-}$ mCCD cells by scanning electron microscopy (SEM). Most cilia in both WT and *Kif13b*$^{-/-}$ cells displayed a membrane invagination/pocket at the base (67.4% and 66.7% of cilia in WT and *Kif13b*$^{-/-}$ cells, respectively; Figure 5a). Ciliary membrane bulging was observed in both WT and *Kif13b*$^{-/-}$ cells and occurred more frequently in *Kif13b*$^{-/-}$ cells compared to WT cells, although the difference was not statistically significant (Figure 5a, b). However, whereas cilia with membrane bulges at the tip were observed at similar frequency in WT and *Kif13b*$^{-/-}$ cells (21.7% ±10% and 19.5% ±7% of cilia, respectively; Figure 5c), membrane bulging along the ciliary shaft was significantly more frequent in cilia of *Kif13b*$^{-/-}$ cells (29.6% ±5% and 17.2% ±8%, respectively; Figure 5c). The size of the membrane bulges observed at the tip and along the shaft of cilia in both WT and *Kif13b*$^{-/-}$ mCCD cells (Figure 5a) is equivalent to or larger than the diameter of the cilium (100 nm), classifying them in the 100-1000 nm size range for large EVs (Doyle and Wang, 2019). These membrane bulges resemble budding EVs previously observed in primary cilia of murine IMCD3, primary biliary epithelial and neuroepithelial cells, as well as Madin-Darby canine kidney (MDCK) and hTERT-RPE1 cells (Dubreuil et al., 2007, Hogan et al., 2009, Chacon-Heszele et al., 2014, Huang et al., 2016, Nager et al., 2017, Sun et al., 2019, Kiesel et al., 2020). Thus, loss of KIF13B in mCCD cells leads to increased membrane bulging along the ciliary shaft, which may be due to delayed EV scission or increased rate of EV budding from this site.

Ciliary localization and function of ZDHHC5

To investigate the mechanism by which KIF13B might regulate the budding or release of EVs from cilia we initially focused on HRS, which was depleted from the 24 h small EVs

from *Kif13b*$^{-/-}$ cells compared to WT (Figure 4a; Table S1), as well as on the ubiquitin E3 ligase ITCH and the palmitoyl transferase ZDHHC5, which were both depleted from the 72 h small EVs (Figure 4b; Table S2). We first performed IFM analysis in our WT, *Kif13b*$^{-/-}$ and rescue mCCD lines to investigate if these proteins localized to the cilium-basal body axis in a KIF13B-dependent manner. For HRS we analyzed 24 h serum-starved cultures, and occasionally observed HRS localization in the vicinity of the basal body (Figure S3a and data not shown). By similar analysis of 72 h serum-starved cultures using an antibody against ITCH, we occasionally observed faint staining of ITCH along the cilium (Figure S3b). However, the weak HRS and ITCH staining intensities at the cilium/basal body precluded meaningful quantitative analysis. In contrast, similar analysis using an antibody against ZDHHC5 showed prominent localization of ZDHHC5 to the basal body and primary cilium and indicated that its ciliary levels are higher at 72 h compared to 24 h of serum starvation (Figure 6a, b). There was a trend towards reduced ciliary levels of ZDHHC5 in the 72 h serum-starved mutant cells compared to controls, but this change was not statistically significant (Figure 6b). Treatment of WT cells with Lomitapide, which is an orphan drug shown to inhibit ZDHHC5 in pancreatic cancer cells (Wang et al., 2023b), did not affect ciliary length (Figure 6c, d), but led to significant ciliary depletion of ARL13B after 24 h of treatment (Figure 6c, e). Since palmitoylation of ARL13B promotes its ciliary targeting and stability (Cevik et al., 2010, Li et al., 2010, Roy et al., 2017), the latter result suggests that ARL13B may be a substrate of ZDHHC5 although more work is needed to confirm this. Combined with our small EV proteomics data (Figure 4b; Table S2), we conclude that ZDHHC5 is localized to cilia where it negatively regulates ciliary length and ARL13B levels, and KIF13B affects ZDHHC5 cellular trafficking and EV release.

ALIX localizes to primary cilia in a KIF13B-dependent manner and controls ciliary PC2 homeostasis

To further investigate the mechanism by which KIF13B might regulate the budding or release of EVs from cilia we next focused on ALIX, given that: 1) ALIX promotes EV release from cilia of *C. reinhardtii* where it localizes to the transition zone (Diener et al., 2015, Long et al., 2016); 2) ALIX is present in both small and large EVs from mCCD cells (Figure S2a, c); 3) TSG101, a direct interactor of ALIX (Strack et al., 2003, von Schwedler et al., 2003) detected in primary cilia of IMCD3 cells (Aslanyan et al., 2023), was significantly reduced in large EVs purified from spent medium from 72 h serum-deprived *Kif13b*$^{-/-}$ cultures compared to WT-derived EVs (Figure S2c, d); and 4) ALIX is a substrate of ITCH (O'Connor et al.,

2015), which was depleted from small EVs of 72 h serum-starved *Kif13b*$^{-/-}$ cells (Figure 4b). Notably, IFM analysis of 24 and 72 h serum-deprived WT, *Kif13b*$^{-/-}$ and rescue mCCD cell lines using antibodies against acetylated α-tubulin and ALIX showed that ALIX is localized at the base of primary cilia in these cells (Figure 7a and data not shown). Quantification of relative ALIX fluorescence staining intensities at the ciliary base of 24 and 72 h serum-deprived cells revealed a significant decline in ciliary ALIX levels in the *Kif13b*$^{-/-}$ cells after 72 h of serum starvation, but not after 24 h of serum starvation, as compared to the WT and rescue lines (Figure 7b). Overall cellular levels of ALIX were not affected in the mutant cells (Figure S1d), indicating that KIF13B specifically affects localization/retention of ALIX at the cilium.

To test if ALIX affects ciliary targeting or homeostasis of PC2 we partially depleted it from mCCD cells using siRNA (Figure 7c) and subjected the cells to 24 or 72 h serum starvation, followed by IFM analysis with antibodies against ciliary markers and PC2. Partial depletion of ALIX did not affect ciliation frequency (Figure 7d) and led to a small, but significant reduction in ciliary length at the 24 h time point as compared to control cells (Figure 7e). Moreover, partial depletion of ALIX caused a significant accumulation of PC2 within cilia after 72 h of serum starvation, as compared to control cells (Figure 7f, g). Thus, ALIX negatively regulates ciliary levels of PC2 in mCCD cells subjected to 72 h of serum starvation.

KIF13B interacts with ITCH, but not with ZDHHC5 and ALIX

Finally, to investigate how KIF13B might affect subcellular localization and/or EV release of ITCH, ZDHHC5 and ALIX, we performed immunoprecipitation experiments to test if KIF13B interacts with these proteins. Indeed, we found that KIF13B co-precipitated with ITCH (Figure S4a), but not with ZDHHC5 or ALIX (Figure S4b, c), suggesting that KIF13B binds specifically to ITCH. Using similar approaches, we also detected an interaction between KIF13B and SCAMP3 (Figure S4c), which is a substrate of ITCH (O'Connor et al., 2015) known to bind TSG101 and HRS (Aoh et al., 2009). Taken together, our immunoprecipitation analysis supports a role for KIF13B in regulating endolysosomal trafficking and EV release of ALIX-TSG101 and ESCRT-0 (HRS-STAM) complex components and suggests that KIF13B may affect these pathways through an interaction with ITCH.

Discussion

Here we show that KIF13B regulates ciliary PC2 homeostasis and EV release in mCCD cells in a time-dependent manner, as summarized in Figure 8. Specifically, we found that in newly formed cilia (24 h serum starvation), KIF13B negatively regulates ciliary PC2 levels, but upon prolonged serum starvation (72 h) to induce cilia maturation, this phenotype is reversed with *Kif13b*$^{-/-}$ cells displaying significantly reduced ciliary levels of PC2 compared to controls. Overall cellular levels of PC2 were not altered in the *Kif13b*$^{-/-}$ cells compared to WT, indicating that loss of KIF13B does not affect the net environmental release or lysosomal degradation of PC2, but rather causes a change in its ciliary localization, intracellular trafficking route(s) and EV release mechanism. Since KIF13B was observed to move within cilia of mCCD cells and appeared to be released from the ciliary tip in large EVs, it is possible that KIF13B and PC2 are co-released in EVs from cilia, which could be tested in future studies via live cell imaging analysis.

The time-dependent changes in ciliary PC2 levels observed in the *Kif13b*$^{-/-}$ cells were paralleled by changes in the overall frequency of release and/or protein content of small vs. large EVs. Specifically, the KIF13B-deficient cells initially release fewer small EVs than WT controls, and these are depleted for HRS and THBS1. Moreover, under these conditions small EVs from both WT and mutant cultures are devoid of PC1/PC2. During prolonged serum starvation *Kif13b*$^{-/-}$ cells gradually increase their EV release frequency, and PC2 release via small EVs increases, suggesting that an adaptive mechanism is upregulated over time in the mutant cells. Furthermore, under these conditions the mutant cilia display increased membrane bulging along the ciliary shaft compared to WT cilia. The reduced ciliary levels of PC2 and increased membrane bulging seen in 72 h serum-starved *Kif13b*$^{-/-}$ cells was correlated with depletion of ALIX from the ciliary base, and partial depletion of ALIX itself led to increased ciliary levels of PC2. Although speculative at this point, one possible interpretation of these results is that ALIX undergoes excessive release or retrieval from the ciliary base in the 72 h serum-starved *Kif13b*$^{-/-}$ cells, and that this in turn causes depletion of PC2 from cilia (Figure 8). In line with this hypothesis, our analyses of large and small EVs from 72 h serum-starved cells suggested that compared to WT cells, *Kif13b*$^{-/-}$ cells release significantly more TSG101 in small EVs as opposed to large EVs, consistent with the ALIX-TSG101 EV biogenesis pathway being dysregulated in the mutant cells. In addition, KIF13B might also affect ciliary EV release and PC2 homeostasis via the HRS-STAM pathway, which is required for downregulating ciliary PC2 levels in *C. elegans* (Hu et al., 2007), since

HRS and STAMBP were depleted from small EVs of KIF13B-deficient cells in a time-dependent manner (Figure 8). In support of a role for KIF13B in regulating the ALIX-TSG101 and HRS-STAM pathways, our immunoprecipitation analyses indicated that KIF13B binds to ITCH, which is known to ubiquitylate several components of these pathways (Aoh et al., 2009).

Another potential regulator of EV release from cilia is the palmitoyl transferase ZDHHC5, which we found to localize to cilia as well as small EVs. Although ciliary levels of ZDHHC5 were largely unaffected by loss of KIF13B, small EVs purified from 72 h serum-starved *Kif13b*$^{-/-}$ cells were significantly depleted for ZDHHC5 compared to WT-derived EVs, suggesting dysregulated endo-lysosomal trafficking of ZDHHC5 in the mutant cells. Notably, palmitoylation is known to regulate EV cargo sorting (Atukorala and Mathivanan, 2021), and several ciliary membrane proteins and known EV cargoes such as ARL13B and PC1 are palmitoylated by an unknown mechanism (Roy and Marin, 2019). Interestingly, inhibition of ZDHHC5 with Lomitapide led to ciliary depletion of ARL13B in mCCD cells, consistent with a role for ZDHHC5 in regulating ciliary membrane protein targeting and/or homeostasis. Moreover, ZDHHC5 was shown to bind the known KIF13B interactor DLG4 (Brigidi et al., 2015, Zhu et al., 2016), suggesting that KIF13B may regulate ZDHHC5 trafficking via DLG4 or related DLGs. It will be interesting to investigate this idea further, as well as to directly address the potential role of ZDHHC5 in regulating palmitoylation, ciliary recruitment and/or EV release of ARL13B and PC1.

In addition to the ALIX-TSG101 pathway and the ESCRT pathway involving HRS-STAM, small EV (exosome) biogenesis and cargo sorting at the membrane of MVBs can also occur via a wedge-driven curvature pathway that relies on the enzyme sphingomyelinase 2 (nSMase2) to remove the head group of sphingomyelin to produce ceramide (Dixson et al., 2023). The latter pathway is inhibited by GW4869 that targets nSMase2 (Trajkovic et al., 2008), and cargoes sorted via this pathway are typically concentrated in membrane microdomains enriched in flotillin and cholesterol (Dixson et al., 2023). Interestingly, our NTA analysis of small EVs purified from untreated and GW4869-treated WT and *Kif13b*$^{-/-}$ cultures after 24 h of serum-starvation showed that GW4869 inhibition has a more dramatic effect on the number on small EVs being released from WT compared to mutant cells, suggesting that the GW4869-sensitive exosome biogenesis pathway is already dysregulated in the *Kif13b*$^{-/-}$ cells. Consistent with this, our MS analysis of small EVs isolated from WT and *Kif13b*$^{-/-}$ cultures after 72 h of serum starvation indicated that proteins involved in

ceramide or cholesterol homeostasis (e.g. ASAH2, ARL4C) are depleted from small EV samples from the mutant cells. Although more experiments will be required to examine the underlying mechanisms, it is tempting to speculate that these include altered CAV1-dependent cholesterol homeostasis, given the known role of KIF13B in promoting CAV1- and LRP1-mediated cholesterol uptake in hepatocytes (Kanai et al., 2014). Furthermore, since KIF13B was shown to regulate ciliary localization of CAV1 and interacted with NPHP4 at the ciliary transition zone (Schou et al., 2017), a more direct role for KIF13B-CAV1-NPHP4 interactions in promoting ciliary membrane homeostasis and EV release can be envisioned. In this context we note that mutations in NPHP4 were shown to affect ciliary EV release in *C. reinhardtii* (Wang et al., 2022) and *C. elegans* (Wang et al., 2023a), and CAV1 was implicated in ciliary PC2 homeostasis in *C. elegans* (Scheidel et al., 2018) and in EV biogenesis in other contexts (Ariotti et al., 2021).

Finally, although the molecular basis for the time-dependent changes in EV release frequency and composition observed in the *Kif13b*$^{-/-}$ cells remains to be clarified, it is notable that previous studies reported that mutations in genes that affect certain endo-lysosomal- or EV biogenesis pathways can lead to upregulation of alternative pathways to maintain cellular homeostasis. For example, mutations in BBS genes that lead to impaired retrograde IFT-mediated retrieval of receptors from cilia were shown to cause excessive release of EVs from the ciliary and periciliary membrane compartments in cultured kidney epithelial cells (Nager et al., 2017, Volz et al., 2021) as well as in *C. elegans* (Akella et al., 2020). Additionally, in *Drosophila* motor neurons, opposing pathways involving RAB4, RAB11 and the retromer complex ensure plasticity of endo-lysosomal- and EV trafficking to maintain cellular homeostasis when key components of one pathway are mutated (Walsh et al., 2021). Unraveling the mechanisms underlying such plasticity will be an important task for future studies and may help explain specific aspects of ADPKD disease pathology as well as other ciliopathies.

Materials and methods

Cell lines and reagents. Cell lines and reagents used in this study are listed in Table 1. Immortalized mCCD were generously provided by Dr. Eric Féraille from University of Lausanne, Switzerland, and have been described previously (Montesano et al., 2009). Human embryonic kidney (HEK) 293T cells were from ATCC (cat. #CRL-3216).

Cell culture conditions. mCCD cells were grown at 37 ^{o}C with 5% humidified CO_2 in DMEM/F12 with GlutaMaX (Thermo Fisher Scientific, cat. #10565018) supplemented with 2% fetal bovine serum (FBS, heat inactivated, Merck), 5 µg/ml insulin (Merck, cat. # I6634), 5 µg/ml holo-transferrin (Merck, cat. #T0665), 5 ng/ml EGF (Merck, cat. #SRP3196), 50 nM dexamethasone (Merck, cat. #D4902), 60 nM sodium selenite (Merck, cat. #S5261), 1 nM 3,3′,5-Triiodo-L-thyronine sodium salt (Merck, cat. #T6397), and 1% penicillin-streptomycin (Merck, cat. #P0781). To promote ciliation, mCCD cells were grown to ca. 80% confluency and then cultured at 37 ^{o}C with 5% humidified CO_2 for 24, 48 or 72 h in DMEM/F12 – GlutaMaX supplemented with 60 nM sodium selenite and 5 µg/ml holo-transferrin. HEK293T cells were cultured as described previously (Rezi et al., 2023).

Generation of *Kif13b*$^{-/-}$ and transgenic mCCD cell lines. To knock out *Kif13b* in mCCD cells we used CRISPR/Cas9 methodology and four sgRNA sequences from the mouse CRISPR "Brie" Knockout Library (Doench et al., 2016). The sequences are provided in Table 1. To generate the Cas9-gRNA plasmids, the sgRNA spacers were cloned into the pSpCas9(BB)-2A-Puro (PX459) V2.0 plasmid (Addgene #62988) as described previously (Ran et al., 2013). Briefly, the complementary sgRNA oligos were phosphorylated and annealed and subsequently ligated into the BbsI-digested backbone. Selected clones were sequenced to verify the spacer sequence. mCCD cells were transfected with the Cas9-gRNA plasmids (a pool of all 4 gRNAs) using reverse transfection with Lipofectamine 3000 (Thermo Fisher Scientific). A day after transfection, cells were treated with 2 µg/ml puromycin (Invitrogen, cat. #A11138-03) for 72 h. After 2-3 passages, cells were tested for KIF13B protein depletion by western blot analysis.

To create rescue lines from the *Kif13b*$^{-/-}$ mCCD pooled parental line, we generated lentiviral expression constructs coding for mNeonGreen-KIF13B or mCherry-KIF13B, expressed under EF1a and IRES promoters to ensure low and stable expression (Aslanyan et al., 2023). In brief, the full-length human *KIF13B* coding sequence was cloned into pENTR-mCherry-C1 or pENTR-mNeonGreen-C1 using standard cloning techniques. The resulting Gateway entry plasmids were further recombined with the pCDH-EF1a-Gateway-IRES-BLAST destination plasmid using the Gateway LR recombination kit (Invitrogen, cat. #11791020). All cloning vectors were kindly supplied by Dr. Kay Oliver Schink, Oslo university Hospital, Norway, and were described in (Campeau et al., 2009). To generate lentiviruses, lentiviral expression plasmids were co-transfected with packaging plasmids pMD2.G and pCMVΔ-R8.2 (kind gift of Dr. Carlo Rivolta, Institute of Molecular and Clinical Ophthalmology

Basel, Switzerland) into HEK293T cells using Lipofectamine 3000 (Thermo Fisher Scientific). Clarified culture medium containing the lentivirus particles was then used to transduce mCCD WT and mCCD *Kif13b*$^{-/-}$ cells. Expressing cells were selected using 15 µg/ml blasticidin and expression was confirmed with western blotting and immunofluorescence microcopy.

Gene silencing with siRNA. Gene silencing of ALIX was performed in mCCD cells using siRNA and Lipofectamine® 3000 (Thermo Fisher Scientific). mCCD WT cells were seeded in DMEM/F12 in 6-well plates at 70-80% confluency. Transfection was performed by combining 40 nM of either ALIX-specific or control siRNA (Table 1) and 7.5 µl Lipofectamine® 3000 (Thermo Fisher Scientific) in 250 µl serum-deprived DMEM/F12 medium and incubated for 15 min at room temperature prior to dropwise addition onto the cells. Subsequently, the media was swirled gently to ensure proper dispersion before the cells were incubated at 37 °C and 5% CO_2. Transfection medium was removed after 24 h and cells were serum starved for either 24 or 72 h before being used for further experiments.

Inhibition of ZDHHC5. Inhibition of ZDHHC5 was done using the small molecule Lomitapide (Medchem Express, cat# HY-14667). Prior to inhibition experiment, WT mCCD cells were seeded on glass coverslips and allowed to reach 80% confluence. Cells were subjected to 24 h serum starvation period using serum-depleted medium, to promote ciliogenesis. After 24 h of starvation the medium was changed to inhibitor-supplemented starvation medium (5 µM Lomitapide or DMSO for the control) and cells were incubated for additional 12 or 24 h. Subsequently, the cells were examined by IFM analysis.

Immunoprecipitation, SDS-PAGE and western blot analysis. Immunoprecipitation in HEK293T cells was carried out using relevant antibody-conjugated beads (see Table1) as described previously (Goncalves et al., 2021) except that the washing buffer contained 0.1% NP-40 instead of 0.5% NP-40. Unless otherwise indicated, SDS-PAGE and western blotting was performed as described previously (Goncalves et al., 2021) by using antibodies and dilutions as listed in Table 1.For western blot analysis of small EVs purified by ultracentrifugation, small EV pellets were resuspended in loading buffer (0.125 M Tris-HCl, 20% (v/v) glycerol, 0.004% (w/v) bromphenol blue) run on a 10% SDS-PAGE and transferred to a PVDF membrane (Immobilon® -FL PVDF membrane, Sigma-Aldrich, cat. #05317). The membrane was blocked with blocking buffer (0.5% Casein; 0.1% Tween; 0.04%NaN_3; 150 mM NaCl) and incubated with primary (overnight, 4°C) and secondary

antibodies (1 h), listed in Table 1. Fluorescence detection was carried out using Odessey Fc Imaging System (LICOR Bioscience).

Immunofluorescence microscopy. Antibodies used in this study and dilutions for IFM are listed in Table 1. For PC2 staining in mCCD cells, we used an IFM protocol method described in (He et al., 2018). Briefly, mCCD cells were grown to ca. 80% confluency and then serum- and hormone-deprived for 24 or 72 h. Cells were first pre-fixed with 0.4% PFA in phosphate-buffered saline (PBS) for 5 min at 37 ^{o}C in a cell culture incubator. Cells were then permeabilized with PHEM buffer (50 mM PIPES; 50 mM HEPES; 10 mM $MgCl_2$; pH 6.9) containing 0.5% Triton X-100 for 2 min at 37 ^{o}C. Permeabilized cells were fixed again in 4% PFA at room temperature for 15 min and blocked in blocking buffer (3% BSA in PBS) for 1 h at room temperature. Cells were then incubated 1-2 h at room temperature or overnight at 4 °C with primary antibodies diluted in blocking buffer. After several washes in PBS, cells were next incubated with secondary antibodies diluted in 2% BSA in PBS for 1 h at room temperature. Finally, nuclei were stained with DAPI (Sigma-Aldrich, cat. #D9542). Coverslips were mounted on slides with Shandon Immu-Mount (Thermo Scientific, cat. #9990402) with 6 % N-propyl gallate (1:12) mounting medium. For ALIX and ZDHHC5 staining, mCCD cells were plated on glass coverslips before the serum starvation and then fixed with 4% PFA for 15 min at room temperature or 20 min at 4 °C followed by permeabilization with 1% BSA and 0.2 % Triton X-100 in PBS for 12 min. The remaining steps were as described for PC2 staining using antibodies and dilutions indicated in Table 1.

Time lapse live cell imaging. To observe KIF13B dynamics in the primary cilia of mCCD cells, we used mCCD cells stably expressing mNeonGreen-KIF13B. The primary cilia were visualized either by SiR-Tubulin staining or by stable expression of mCherry-RAB8A (Aslanyan et al., 2023). Cells were grown on a 35 mm glass-bottom dish and serum-starved for 24-72 h. For staining with SiR-tubulin dye (Cytoskeleton, Inc., cat. #CY-SC002), culture medium was supplemented with 1 µM of SiR-tubulin, dissolved in DMSO, and incubated in a cell incubator at 37 °C in a humidified atmosphere containing 5% CO_2 for at least 30 min prior to cell imaging. All imaging was performed in a humidity chamber on an Olympus inverted microscope (IX83) equipped with Yokogawa spinning disc with 100× oil objective, as described previously (Aslanyan et al., 2023). The cells starved for 24-48 h were imaged using the wide-field or confocal settings, at 5-10 sec time intervals, while cells starved for 72 h were imaged using the confocal settings, at 3 sec time intervals.

.

Purification of extracellular vesicles. We applied two alternative methods to purify EVs. To purify small EVs for NTA, TEM and MS analysis we used a previously published ultracentrifugation approach (Volz et al., 2021). Briefly, spent medium was collected from 24, 48 or 72 h serum-starved mCCD cultures and first centrifuged at 1,000 x g for 10 min to remove cell debris. The supernatant was collected and subjected to further centrifugation at 10,000 x g for 30 min at 4 ^{o}C to sediment large EVs and particles. The supernatant was then subjected to ultracentrifugation at 100,000 x g for 2 h at 4 °C to sediment small EVs (Optima L-80K ultracentrifuge, Beckman Coulter, swing bucket SW28 rotor or Optima MAX-E ultracentrifuge, Beckmann Coulter, TLA-55 fixed-angle rotor). The final pellet was resuspended in particle-free PBS, Laemmli buffer or 6 M Urea-Tris buffer and used for downstream analyses.

To purify large and small EV for western blot analysis (Figure S2), we used a combined centrifugation and lectin-mediated precipitation approach (Samsonov et al., 2016). Spent medium from 72 h serum-deprived mCCD cultures was first centrifuged at 3,000 x *g* for 30 min to remove cell debris. The supernatant was then centrifuged for 40 min at 10,000 x *g* to sediment large EVs, which were collected, resuspended in PBS supplemented with protease inhibitor and centrifuged again for 60 min at 20,000 x *g* prior to SDS-PAGE and western blot analysis. Meanwhile, 1 µg/ml Concanavalin A from *Canavalia ensiformis* (Sigma-Aldrich, cat. # C2010) was added to the supernatant and the mixture put on slow stir for 16 h at 4 □. Subsequently, small EVs were collected by centrifugation for 60 min at 14,000 x *g*. The pellet was resuspended in PBS supplemented with protease inhibitor and centrifuged again for 60 min at 20,000 x *g* prior to SDS-PAGE and western blot analysis.

Scanning electron microscopy (SEM). To prepare the samples for SEM imaging, mCCD cells grown on glass coverslips and serum starved for 72 h were fixed in 2% glutaraldehyde in 100 mM Sodium cacodylate at room temperature for at least 2 h up to several days. Subsequently, cells were washed three times in 100 mM sodium cacodylate and then treated with 1% OsO_4 in 100 mM sodium cacodylate for 1-2 h at room temperature. The cells were then washed with deionized water and dehydrated with a graded series of ethanol solutions (30%, 50%, 70%, 80%, 95%, and 100%) at room temperature, with each step lasting 5-10 min. The samples were allowed to dry using a critical point drier. Dried samples were mounted onto stubs and sputter coated with 6 nm gold. The coated samples were then placed

into a SEM chamber and images captured with a FEI Quanta 3D FEG dual beam SEM microscope (University of Copenhagen´s Core Facility for Integrated Microscopy).

Transmission electron microscopy (TEM) of small EVs. Small EV pellets isolated by ultracentrifugation from spent media of mCCD cells following 48 h serum-starvation were resuspended in particle-free PBS. They were subsequently applied to 400 mesh carbon-coated copper grids (Electron Microscopy Science) and allowed to settle for 1 minute. Embedded EVs were fixed with 1% glutaraldehyde for 5 min and washed four times with deionized water (ddH_2O). Negative staining was performed by applying 2% uranyl acetate for 1 min and the grids were allowed to dry. Imaging was done with a FEI Tecnai G2 12 BioTwin transmission electron microscope (Fei, Company, Hillsboro, USA).

Nanoparticle tracking analysis (NTA)

Small EVs were isolated by ultracentrifugation from spent media of 24, 48 and 72 h serum-deprived mCCD cells. Inhibition of EV release was performed by treatment with 10 µM GW4869 (Sigma-Aldrich, cat. #D1629) dissolved in DMSO during serum starvation (24 h) prior EV preparation. Particles were resuspended in particle-free PBS and measured using ZetaView Nanoparticle Analyzer PMX-230 (TWIN) (Particle Metrix). Particle movement was recorded in scatter mode 1-2 Cycles at 11 Positions, at a steady temperature of 25°C and analysed using the Software ZetaView (version 8.05.16 SP3).

Mass spectroscopy

Small EV pellets from spent medium of serum-deprived mCCD cells (n=4/cell line, 24 h and 72 h) were isolated using ultracentrifugation. Pellets were diluted in 6 M Urea-Tris buffer (0.4 M Tris pH 7.8; 6 M Urea) and subjected to liquid chromatography-MS analysis as described previously (Volz et al., 2021).

GO term enrichment analysis. To conduct the analysis, the GetGO (Boldt et al., 2016) online analysis tool (min. count: 4) was performed for the Tier 1 proteins of the KIF13B EVome dataset, as described above. Subsequently, the acquired GO terms and their ratio were visualized using the ggplot2 package in R (Wickham, 2016).

Statistical analysis

Quantitative and statistical analysis of the IFM data was done as described previously (Goncalves et al., 2021). For western blot analysis we utilized the UN-SCAN-IT gel v6.1

analysis software to measure the average pixel intensity of the bands. Subsequently, we normalized the acquired numbers to the loading control and performed the statistical analysis in GraphPad Prism 10. All quantitative data are presented as mean ± standard deviation. Differences were considered significant when the p-value was <0.05. Unless otherwise stated, the results were confirmed in at least three independent biological replicates. Statistical analysis on NTA data was done in Graphpad Prism 7.0 software (Graphpad Software Inc.). Outliers were excluded using the ROUT method (Q = 1%). Gaussian distribution was tested using Shapiro-Wilk and Kolmogorov-Smirnov test ($P < 0.05$). For Gaussian distributed data, *t* test and for non-Gaussian distributed data, Mann-Whitney *U* test performed. Significance levels: $P > 0.05$ not significant (ns), $P \leq 0.05$ *, $P \leq 0.01$ **, $P \leq 0.001$ ***, $P \leq 0.0001$ ****.

Acknowledgements

We are grateful to Feng Qian and the Polycystic Kidney Disease Research Resource Consortium (U54DK126114) for providing the anti-PC2 (rabbit polyclonal) antibody, and to Eric Féraille, Kay Oliver Schink, Carlo Rivolta and Yuko Mimori-Kiyosue for other reagents. This work was supported by grants NNF18SA0032928 and NNF22OC0080406 from the Novo Nordisk Foundation (LBP), grant 2032-00115B from the Independent Research Fund Denmark (LBP), and the European Union's Horizon 2020 research and innovation program Marie Sklodowska-Curie Innovative Training Networks (ITN) grant 861329 (LBP, STC, KB).

Author contributions

CKR, AF, JL, GL, SLJ, JKTS, AS, CRB, FC, KB, and ZA performed experiments; CKR, AF, JL, GL, CRB, FC, KB, MC and ZA analyzed data; CKR, AF, CRB, FC, STC, KB, MC, ZA and LBP prepared the figures; ZA and LBP conceived the project and wrote the paper with input from all authors. ZA, LBP, STC, KB and HMS obtained funding for the study.

Table 1. Cell lines, reagents, and plasmids used in this study.

Reagent type (species) or resource	Designation	Source or reference	Identifiers	Additional information
Cell line (*Mus musculus*)	mCCD	Eric Féraille lab, University of Lausanne, Switzerland	Wild type (parental)	
Cell line (*M. musculus*)	mCCD *Kif13b*$^{-/-}$	This study	Pool	Generated by CRISPR/Cas9 methodology
Cell line (*M. musculus*)	mCCD/mNG-KIF13B	This study	Pool	Generated by lentiviral transduction
Cell line (*M. musculus*)	mCCD/mNG-KIF13B/mCherry-Rab8	This study	Pool	Generated by lentiviral transduction
Cell line (*M. musculus*)	mCCD *Kif13b*$^{-/-}$/mCherry-KIF13B	This study	Pool/rescue line	Generated by lentiviral transduction
Cell line (*M. musculus*)	mCCD *Kif13b*$^{-/-}$/mNG-KIF13B	This study	Pool/rescue line	Generated by lentiviral transduction
Cell line (*Homo sapiens*)	HEK293T	ATCC	Cat# CRL-3216	
Strain, strain background (*Escherichia coli*)	DH10B	Lab stock	N/A	
Antibody	Anti-acetylated alpha-tubulin (mouse monoclonal)	Sigma-Aldrich	Cat# T7451	IFM (1:2000) WB (1:5000)
Antibody	Anti-acetylated alpha-tubulin (rabbit monoclonal)	Abcam	Cat# ab179484	IFM (1:2000)
Antibody	Anti-AIP1 (ALIX; mouse monoclonal)	BD Transduction Laboratories	Cat# 611620	WB (1:1000)

Antibody	Anti-ALIX (rabbit polyclonal)	Merck/Sigma-Aldrich	Cat# ABC40	IFM (1:1000) WB (1:3000)
Antibody	Anti-alpha-tubulin (mouse monoclonal)	Sigma-Aldrich	Cat# T5168	WB (1:10000)
Antibody	Anti-ARF6 (rabbit polyclonal)	Abcam	Cat# ab77581	WB (1:400) Antibody discontinued by manufacturer
Antibody	Anti-ARL13B (rabbit polyclonal)	Proteintech	Cat# 17711-1-AP	IFM (1:600) WB (1:600)
Antibody	Anti-CD81 (mouse monoclonal)	Santa Cruz Biotechnology	Cat# sc-166029	WB (1:1000)
Antibody	Anti-CD9 (rat monoclonal)	BD Transduction Laboratories	Cat# 553758	WB (1:1000)
Antibody	Anti-DTNB (rabbit polyclonal)	Invitrogen	Cat# PA5-63950	WB (1:500)
Antibody	Anti-FLAG (mouse monoclonal)	Sigma-Aldrich	Cat. #F1804	WB (1:1000)
Antibody	Anti-FLOT1 (rabbit polyclonal)	Sigma	Cat# F1180	WB (1:1000)
Antibody	Anti-GAPDH (rabbit polyclonal)	Cell Signalling Technology	Cat# 2118	WB (1:1000)
Antibody	Anti-GFP (rabbit polyclonal)	Sigma	Cat# SAB4301138	WB (1:500)
Antibody	Anti-GM130 (mouse monoclonal)	BD Transduction Laboratories	Cat# 610823	WB (1:1000)
Antibody	Anti-HA (rabbit polyclonal)	Santa Cruz Biotechnology	Cat#sc-805	WB (1:500)
Antibody	Anti-HRS (rabbit polyclonal)	Proteintech	Cat# 10390-1-AP	IFM (1:200) WB (1:500)
Antibody	Anti-HSP70 (mouse monoclonal)	BD Transduction Laboratories	Cat# 610608	WB (1:1000)
Antibody	Anti-ITCH (rabbit	ThermoFischer	Cat# PA5-65539	IFM (1:200) WB (1:500)

	polyclonal)	Scientific		
Antibody	Anti-KIF13B (mouse monoclonal)	Merck	Cat# SAB1412812	WB (1:600)
Antibody	Anti-Mouse IgG 680	LI-COR Bioscience	Cat# 925-68072	Secondary antibody WB (1:10000)
Antibody	Anti-Mouse IgG 800	LI-COR Bioscience	Cat# 925-32212	Secondary antibody WB (1:10000)
Antibody	Anti-Myc (mouse monoclonal)	Cell Signaling Technology	Cat# 2276	WB (1:1000)
Antibody	Anti-PC2 (rabbit polyclonal)	PKD Research Resource Consortium	N/A	IFM (1:1000) WB (1:600)
Antibody	Anti-PC2 (mouse monoclonal)	Santa Cruz	Cat# sc-28331	IFM (1:500) WB (1:1000)
Antibody	Anti-Rabbit IgG 680	LI-COR Bioscience	Cat# 925-68073	Secondary antibody WB (1:10000)
Antibody	Anti-Rat IgG 680	Thermo Fisher Scientific	Cat# A-21096	Secondary antibody WB (1:10000)
Antibody	Anti-SCAMP3 (rabbit polyclonal)	Sigma	Cat# HPA071167	WB (1:500)
Antibody	Anti-TSG101 (mouse monoclonal)	Gene Tex	Cat# GTX70255	WB (1:1000)
Antibody	Anti-ZDHHC5 (rabbit polyclonal)	Proteintech	Cat# 21324-1-AP	IFM (1:100)
Chemical Reagent	GW4869	Sigma	Cat# D1629	Dissolved in DMSO and used in 10 µM final concentration
Chemical Reagent	Lipofectamine 3000	Thermo Fisher Scientific	Cat# L3000015	
Chemical Reagent	SiR-tubulin	Cytoskeleton, Inc.	Cat# CY-SC002	Dissolved in DMSO and used at 1 M final concentration
Chemical Reagent	Lomitapide	Medchem Express	Cat# HY-14667	Dissolved in DMSO and used at 5 M final concentration
Sequence-based reagent	*M. musculus Kif13b* exon 17 sgRNA	Eurofins Genomics	sgRNA 1	caccgAGGAGAGCCGGTCCACACCG aaacCGGTGTGGACCGGCTCTCCTc
Sequence-based reagent	*M. musculus Kif13b* exon 20 sgRNA	Eurofins Genomics	sgRNA 2	caccgTAACTTCACGTCATAAAACA aaacTGTTTTATGACGTGAAGTTAc

Sequence-based reagent	*M. musculus Kif13b* exon 8 sgRNA	Eurofins Genomics	sgRNA 3	caccgATCATACAGAGTATGTGTCA aaacTGACACATACTCTGTATGATc
Sequence-based reagent	*M. musculus Kif13b* exon 25 sgRNA	Eurofins Genomics	sgRNA 4	caccgGACATTCTCGTGGATCTTAG aaacCTAAGATCCACGAGAATGTCc
Sequence-based reagent	*M. musculus* Control siRNA	Eurofins Genomics	Control siRNA	GCC AUA GAG AUA AGG UAA GAA TT
Sequence-based reagent	*M. musculus* ALIX siRNA	Eurofins Genomics	ALIX siRNA	AAU CUG AUC AUA AUA CCU CAG TT
DNA plasmid	pEGFP-N1	BD Biosciences Clontech		Plasmid discontinued by manufacturer
DNA plasmid	*H. sapiens* KIF13B/pcDNA3	(Lamason et al., 2010)		Codes for HA-KIF13B; used as PCR template to generate mCherry- and mNG-KIF13B fusions
DNA plasmid	*H. sapiens* Δmotor-KIF13B-HA/pcDNA3	(Lamason et al., 2010)		Codes for HA-tagged motorless KIF13B; used for immunoprecipitation experiments
DNA plasmid	*H. sapiens* Δmotor-KIF13B-eGFP/pcDNA3	(Lamason et al., 2010)		Codes for GFP-tagged motorless KIF13B; used for immunoprecipitation experiments
DNA plasmid	*H. sapiens* KIF13B aa 561-1826/pEGFP-C1	(Morthorst et al., 2022)	GFP-KIF13B-Tail 6	Codes for GFP-KIF13B residues 561-1826, used for immunoprecipitation experiments
DNA plasmid	*Rattus norvegicus* DLG1/pEGFP-C1	(Wu et al., 1998)	eGFP-DLG1	Codes for GFP-tagged rat DLG1 (UniProt A0A8I6A5M7), used for immunoprecipitation experiments (positive control)
DNA plasmid	*H. sapiens* ERp57/pcDNA3	(Appenzeller-Herzog et al., 2008)		Codes for HA-tagged ERp57; used for immunoprecipitation experiments as negative control
DNA plasmid	*M. musculus* ITCH/pCINeo-Myc	(Magnifico et al., 2003); Addgene	Plasmid #11427	Codes for Myc-tagged ITCH, used for immunoprecipitation experiments
DNA plasmid	*M. musculus* DHHC5/pNeo-Flag	(Tian et al., 2015); Addgene	Plasmid #85812	Codes for Flag-tagged ZDHHC5, used for immunoprecipitation experiments
DNA plasmid	Rab8A/Tag-RFP-T	Dr Yuko Mimori-		

		Kiyosue (RIKEN Center for Life Science Technologies (CLST), Kobe, Japan)		
DNA plasmid	pSpCas9(BB)-2A-Puro (PX459) V2.0	Addgene	Plasmid # 62988	
DNA plasmid	PX459/*M. musculus Kif13b* guide 1 targeting exon 17	This study	LBP lab plasmid # 943	
DNA plasmid	PX459/*M. musculus Kif13b* guide 2 targeting exon 20	This study	LBP lab plasmid # 944	
DNA plasmid	PX459/*M. musculus Kif13b* guide 3 targeting exon 8	This study	LBP lab plasmid # 945	
DNA plasmid	PX459/*M. musculus Kif13b* guide 4 targeting exon 25	This study	LBP lab plasmid # 946	
DNA plasmid	pENTR20-mCherry-C1 (Gateway)	(Campeau et al., 2009)		
DNA plasmid	pENTR20-mNG-C1 (Gateway)	(Campeau et al., 2009)		
DNA plasmid	pCDH-EF1A-GW-IRES-blast (Gateway)	(Campeau et al., 2009)		
DNA plasmid	pCDH-EF1A-GW-IRES-neo (Gateway)	(Campeau et al., 2009)		
DNA plasmid	pMD2.G	Carlo Rivolta, Institute of Molecular and Clinical Ophthalmol		

		ogy Basel, Switzerland		
DNA plasmid	pCMVΔ-R8.2	Carlo Rivolta, Institute of Molecular and Clinical Ophthalmology Basel, Switzerland		
DNA plasmid	mCherry-KIF13B/ pCDH-EF1A-GW-IRES-blast	This study	LBP lab plasmid # 1060	Codes for mCherry-KIF13B
DNA plasmid	mNG-KIF13B/pCDH-EF1A-GW-IRES-blast	This study	LBP lab plasmid # 1056	Codes for mNG-KIF13B
Other	GFP-Trap Agarose	ChromoTek GmbH	Cat# gta-20	
Other	Pierce™ Anti-HA Agarose	ThermoFisher	Cat# 26182	

Figure legends

Figure 1. Ciliary PC2 localization in WT, *Kif13b*$^{-/-}$ and rescue mCCD cell lines. (**a**) Western blots of WT and *Kif13b*$^{-/-}$ mCCD cells grown with (+) or without (-) FBS for 24 h; blots were probed with antibodies as indicated; α-tubulin (α-tub) serves as loading control. Molecular mass markers are shown in kDa to the left. (**b**) Quantification of relative cellular PC2 levels in WT and *Kif13b*$^{-/-}$ cells after 24 h of serum starvation, based on western blots as shown in panel a (n=3). (**c**) IFM analysis of indicated mCCD cell lines after 24 h serum starvation. Acetylated α-tubulin (AcTub; blue) marks the ciliary axoneme (arrowheads) and PC2, stained with an antibody described in (He et al., 2018), is shown in green. The ciliary base is marked with asterisk. Insets show enlargement of the cilium-centrosome axis, and the rightmost panels are 3D renderings thereof. mCh-KIF13B: mCherry-KIF13B. (**d**) Quantification of relative ciliary PC2 staining intensities of the indicated mCCD cell lines, based on images as shown in (c). (**e**) IFM analysis of indicated mCCD cell lines following serum starvation for 24 or 72 h and using commercially available antibodies against PC2 (green) and acetylated α-tubulin (AcTub; magenta). (**f**) Quantification of relative ciliary PC2 staining intensity in the indicated mCCD cell lines, based on images as shown in (e). For quantifications in (d, f) background-corrected mean fluorescence intensity (MFI) of PC2 was measured for 50 cilia per cell line per experiment and normalized to that of WT 24 h mean value (n=3). *, $p<0.05$; **, $p<0.01$; ****, $p<0.0001$; ns, not significant.

Figure 2. KIF13B movement in cilia of mCCD cells. Montage based on Movie 2 showing mNG–KIF13B (green) transiently moving into the cilium of an mCCD cell that was serum-starved for 72 h. The cilium is marked with SiR-tubulin (magenta). Within 2 minutes, mNG–KIF13B accumulates in the cilium, and some is released from the ciliary tip (arrowheads). Scale bar 2µm.

Figure 3. Characterization of small EVs from WT and *Kif13b*$^{-/-}$ mCCD cell cultures. (**a**) Scheme of procedure used for purification of small EVs from spent cell culture medium. (**b**) Negative staining and TEM analysis of small EVs purified from spent cell culture medium after 48 h of serum starvation (scale bars, 100 nm). (**c**) NTA profiling of small EVs from spent cell culture medium collected after 24, 48, and 72 h of serum starvation, respectively. Data are represented as mean values, error bars show SEM (n=5-6 per cell line per condition). (**d**) Relative increase in small EV release of WT and *Kif13b*$^{-/-}$ cultures at time point 48 and 72 h serum starvation, respectively, compared to the 24 h time point. Based on

data shown in (c). (**e**, **f**) NTA profiling of small EVs purified from spent medium of 24 h serum-deprived WT and *Kif13b*$^{-/-}$ mCCD cell cultures incubated with (+) or without (-) 10 μM GW4869 for 24 h prior to collection of the spent medium (n=14 for untreated; n=7 for GW4869; n=3 for Medium, n=10 for PBS). Data are represented as mean values of particles 50-150 nm in size. Error bars in (e) show SEM. *, p<0.05; **, p<0.01; ***, p<0.001; ns, non-significant.

Figure 4. Composition of small EVs from WT and *Kif13b*$^{-/-}$ mCCD cell cultures. (**a**, **b**) Scatterplots comparing the protein content of small EVs isolated from WT and *Kif13b*$^{-/-}$ mCCD cells after 24 h (**a**) and 72 h (**b**) of serum starvation, based on MS analysis of 4 experimental replicates per condition. Selected proteins that differ significantly in abundance between mutant and WT samples are highlighted. (**c**, **d**) Gene Ontology (GO) enrichment analysis for cellular component (**c**) and molecular function (**d**) for proteins significantly depleted from small EVs of *Kif13b*$^{-/-}$ mCCD cell cultures after 72 h of serum starvation. The tables show the GO terms that are significantly enriched (Fisher's exact test value ≤0.05), listed according to their enrichment ratio. (**e**) List of proteins significantly altered in abundance in small EVs of *Kif13b*$^{-/-}$ mCCD cell cultures after 72 h of serum starvation. Proteins in bold were previously shown to be significantly enriched in small EVs derived from *Bbs4* and/or *Bbs6* mutant kidney epithelial cells (Volz et al., 2021); except for TGM2, all of these proteins were depleted from the *Kif13b* mutant EVs compared to WT.

Figure 5. Ciliary morphology of mCCD cell lines. (**a**) Representative images of different cilia morphologies observed by SEM of WT and *Kif13b*$^{-/-}$ mCCD cells following 72 h of serum starvation. Scale bars, 1 μm. (**b**, **c**) Quantification of ciliary membrane bulges based on SEM images as in (a), with 29-77 cilia analyzed per cell line per experiment (n=4; 163 and 208 cilia analyzed in total for WT and *Kif13b*$^{-/-}$ cells, respectively). *, p<0.05; ns, non-significant.

Figure 6. Ciliary localization and function of ZDHHC5. (**a**, **b**) Representative IFM images (**a**) and quantification of relative ciliary levels of ZDHHC5 (**b**) in indicated mCCD cell lines serum-starved for 24 or 72 h and stained with antibodies against acetylated α-tubulin (AcTub; red) and ZDHHC5 (green). mCh-KIF13B, mCherry-KIF13B. Between 40-50 cilia were measured per condition per experiment (n=3) and the MFI of ciliary ZDHHC5 staining intensity normalized to the mean MFI for WT at 24 h. (**c-e**) Representative IFM images (**c**) and quantification of ciliary length (**d**) and relative ciliary levels of ARL13B (**e**) in 24 h

serum-starved WT mCCD cells treated with vehicle alone (DMSO, Ctrl) or 5 μM Lomitapide for additional 12 or 24 h in serum starvation medium and stained with antibodies against acetylated α-tubulin (AcTub; red) and ARL13B (green). Between 50-60 cilia were measured per condition per experiment (n=3) and the MFI of ciliary ARL13B staining intensity normalized to the mean MFI for DMSO. **, p<0.01; ****, p<0.0001.

Figure 7. Ciliary localization and function of ALIX. (**a**) Representative IFM images of cilia in indicated mCCD cell lines after 72 h of serum starvation and staining with antibodies against acetylated α-tubulin (AcTub; red) and ALIX (green). mCh-KIF13B, mCherry-KIF13B. (**b**) Quantification of relative ALIX level at the ciliary base in the indicated mCCD cell lines subjected to 24 or 72 h of serum starvation, based on images as shown in (a). Rescue corresponds to the *Kif13b*$^{-/-}$ line stably expressing either mNeonGreen-KIF13B or mCherry-KIF13B. MFI of ALIX was measured for 40-50 cilia per cell line per experiment and normalized to that of WT mean (n=5 for the 72 h time points; n=2 for the 24 h time point). (**c**) Western blot analysis (upper panel) of mCCD cells treated with siRNA against ALIX (siALIX) or control siRNA (siCtrl) and subjected to 24 or 72 h of serum starvation, as indicated. Blots were probed with antibodies against ALIX or GAPDH (loading control). The lower panel shows quantification of relative cellular ALIX levels under the indicated conditions (n=3). (**d, e**) Ciliary frequency (**d**) and length (**e**) of siCtrl- and siALIX-treated mCCD cells after 24 or 72 h of serum starvation was determined based on IFM analysis as shown in Figure 6f (n=3), analyzing at least 100 cells per condition per experiment for ciliary frequency, and 40-50 cilia per condition per experiment for ciliary length (n=3). (**f**, **g**) Representative IFM images (**f**) and relative ciliary PC2 levels (**f**) of siCtrl- and siALIX-treated mCCD cells after 24 or 72 h of serum starvation and staining with antibodies against ARL13B and PC2. MFI of PC2 in cilia was measured for 40-50 cilia per condition per experiment and normalized to that of mean value for siCtrl at 24 h (n=3). *, p<0.05; **, p<0.01; ***, p<0.001; ****, p<0.0001; ns, not significant.

Figure 8. Summary of results and working model for how KIF13B affects ciliary PC2 homeostasis and EV release in mCCD cells. After 24 h of serum starvation, *Kif13b*$^{-/-}$ cells release fewer small EVs that WT cells and display increased ciliary levels of PC2, which could be due to reduced release of PC2-containing large EVs from the ciliary tip and/or impaired HRS-dependent endo-lysosomal trafficking. After 72 h of serum starvation, *Kif13b*$^{-/-}$ cells release increased amounts of small EVs with altered composition, display reduced ciliary levels of PC2 and ALIX (represented by light blue shading of the transition zone), and

increased membrane bulging from the side of the cilium, which could be due to impaired release of large EVs from the ciliary tip and upregulated ALIX-dependent release of PC2-containing small EVs from the ciliary base.

Movie 1. Burst-like intraciliary movement of mNeonGreen-KIF13B in live mCCD cells starved for 24-48 h. Representative live cell imaging of *Kif13b*$^{-/-}$ mCCD cells stably expressing mNeonGreen-KIF13B. Cells were serum starved for 24-48 h and stained with SiR-tubulin (magenta) to view the ciliary axoneme and microtubule cytoskeleton. Transient accumulation of mNeonGreen-KIF13B was observed in 15 out of 72 cilia (21%) imaged by this approach.

Movie 2. Burst-like intraciliary movement and tip shedding of mNeonGreen-KIF13B in live mCCD cells starved for 72 h. Representative live cell imaging of *Kif13b*$^{-/-}$ mCCD cells stably expressing mNeonGreen-KIF13B. Cells were serum starved for 72 h and stained with SiR-tubulin (magenta) to view the ciliary axoneme and microtubule cytoskeleton. Transient accumulation of mNeonGreen-KIF13B was observed in 10 out of 30 cilia (33%) imaged by this approach.

Figure S1. Characterization of WT, *Kif13b* mutant and rescue mCCD cell lines. Related to Figures 1-7. (**a**) Representative IFM images of 72 h serum-deprived WT and *Kif13b*$^{-/-}$ cells, stained with anti-acetylated α-tubulin (AcTub) antibody to mark cilia. (**b**) Measurement of ciliation frequency in 24 or 72 h serum-deprived WT and *Kif13b*$^{-/-}$ cells, based on IFM images as in (a). (**c**) Quantification of ciliary length in 72 h serum-deprived WT and *Kif13b*$^{-/-}$ cells, based on SEM images as shown in Figure 5a. Between 23-50 cilia were measured per condition per experiment (n=3). ns, not significant. (**d**) Western blot analysis of lysates from the indicated mCCD cells lines subjected to serum starvation for 24, 48, or 72 h, as indicated, and probed with antibodies specific for the proteins listed on the right; molecular mass markers are shown in kDa to the left. (**e**) Western blots of indicated cell lines using antibodies against KIF13B and α-tubulin (α-tub; loading control). Molecular mass markers are shown in kDa to the left. mNG-KIF13B: mNeonGreen-KIF13B. (**f**) IFM analysis of *Kif13b*$^{-/-}$ cells stably expressing mCherry-KIF13B or mNeonGreen-KIF13B after 24 h of serum starvation. The cells were stained with antibody against acetylated α-tubulin (AcTub). Cells expressing mCherry-KIF13B were additionally stained with an antibody against mCherry (red). Images to the right show enlarged regions of the boxed areas. Note that the KIF13B fusion proteins are concentrated at both centrioles at the base of primary cilia.

Figure S2. Western blot analysis of small and large EVs from WT and *Kif13b*$^{-/-}$ mCCD cell cultures. Related to Figures 3-7. (**a**) Western blot analysis of small EVs purified from spent medium of 48 h serum starved cultures by ultracentrifugation. Blots were probed with antibodies as indicated. Molecular mass markers are shown in kDa to the left. (**b**) Scheme of procedure used for purification of large EVs and small EVs using centrifugation and lectin-mediated precipitation. (**c**) Large EVs and lectin-purified small EVs purified from spent medium of 72 h serum starved cultures were analyzed by western blotting using antibodies as indicated (AcTub, acetylated α-tubulin). Whole cell lysates are included for comparison, and molecular mass markers are indicated in kDa to the left. (**d**) Quantification of the relative distribution of the indicated proteins in large and small EVs, based on western blots as in (c), n=4. *, $p<0.05$; **, $p<0.01$; ns, non-significant.

Figure S3. IFM analysis of HRS and ITCH in serum-starved mCCD cells lines. Related to Figure 3. The indicated cell lines were stained with antibodies against HRS (green) in (**a**) or ITCH (green) in (**b**) as well as anti-acetylated tubulin (AcTub; magenta or red), which marks the cilia. Magnified (2x) and shifted views of the boxed area are shown in the insets. The ciliary base is indicated with asterisks. Note the faint staining of HRS near the ciliary base in panel (a), and the faint staining of ITCH along the cilium-basal body axis in panel (b).

Figure S4. KIF13B interacts with ITCH and SCAMP3 but not with ALIX and ZDHHC5. HEK293T cells were transfected with plasmids coding for the fusion proteins indicated above the lanes, as well as plasmids coding for Myc-ITCH (**a**) or Flag-ZDHHC5 (**b**). The GFP-KIF13B tail 6 (T6) plasmid used in (**c**) codes for the cargo-binding region of KIF13B (residues 561-1826; (Morthorst et al., 2022). Transfected cells were lysed and subjected to immunoprecipitation (IP) with anti-GFP (**a, c**) or anti-HA (**b**) beads, and IP pellets and input samples were analyzed by SDS-PAGE and western blotting with antibodies against relevant proteins, as indicated to the right of the blots. Molecular mass markers are shown in kDa to the left.

References

AKELLA, J. S. & BARR, M. M. 2021. The tubulin code specializes neuronal cilia for extracellular vesicle release. *Dev Neurobiol,* 81**,** 231-252.

AKELLA, J. S., CARTER, S. P., NGUYEN, K., TSIROPOULOU, S., MORAN, A. L., SILVA, M., RIZVI, F., KENNEDY, B. N., HALL, D. H., BARR, M. M. & BLACQUE, O. E. 2020. Ciliary Rab28 and the BBSome negatively regulate extracellular vesicle shedding. *Elife,* 9.

ANSLEY, S. J., BADANO, J. L., BLACQUE, O. E., HILL, J., HOSKINS, B. E., LEITCH, C. C., KIM, J. C., ROSS, A. J., EICHERS, E. R., TESLOVICH, T. M., MAH, A. K., JOHNSEN, R. C., CAVENDER, J. C., LEWIS, R. A., LEROUX, M. R., BEALES, P. L. & KATSANIS, N. 2003. Basal body dysfunction is a likely cause of pleiotropic Bardet-Biedl syndrome. *Nature,* 425**,** 628-33.

ANVARIAN, Z., MYKYTYN, K., MUKHOPADHYAY, S., PEDERSEN, L. B. & CHRISTENSEN, S. T. 2019. Cellular signalling by primary cilia in development, organ function and disease. *Nat Rev Nephrol,* 15**,** 199-219.

AOH, Q. L., CASTLE, A. M., HUBBARD, C. H., KATSUMATA, O. & CASTLE, J. D. 2009. SCAMP3 negatively regulates epidermal growth factor receptor degradation and promotes receptor recycling. *Mol Biol Cell,* 20**,** 1816-32.

APPENZELLER-HERZOG, C., RIEMER, J., CHRISTENSEN, B., SORENSEN, E. S. & ELLGAARD, L. 2008. A novel disulphide switch mechanism in Ero1alpha balances ER oxidation in human cells. *EMBO J,* 27**,** 2977-87.

ARIOTTI, N., WU, Y., OKANO, S., GAMBIN, Y., FOLLETT, J., RAE, J., FERGUSON, C., TEASDALE, R. D., ALEXANDROV, K., MEUNIER, F. A., HILL, M. M. & PARTON, R. G. 2021. An inverted CAV1 (caveolin 1) topology defines novel autophagy-dependent exosome secretion from prostate cancer cells. *Autophagy,* 17**,** 2200-2216.

ASLANYAN, M. G., DOORNBOS, C., DIWAN, G. D., ANVARIAN, Z., BEYER, T., JUNGER, K., VAN BEERSUM, S. E. C., RUSSELL, R. B., UEFFING, M., LUDWIG, A., BOLDT, K., PEDERSEN, L. B. & ROEPMAN, R. 2023. A targeted multi-proteomics approach generates a blueprint of the ciliary ubiquitinome. *Front Cell Dev Biol,* 11**,** 1113656.

ATUKORALA, I. & MATHIVANAN, S. 2021. The Role of Post-Translational Modifications in Targeting Protein Cargo to Extracellular Vesicles. *Subcell Biochem,* 97**,** 45-60.

BOLDT, K., VAN REEUWIJK, J., LU, Q., KOUTROUMPAS, K., NGUYEN, T. M., TEXIER, Y., VAN BEERSUM, S. E., HORN, N., WILLER, J. R., MANS, D. A., DOUGHERTY, G., LAMERS, I. J., COENE, K. L., ARTS, H. H., BETTS, M. J., BEYER, T., BOLAT, E., GLOECKNER, C. J., HAIDARI, K., HETTERSCHIJT, L., IACONIS, D., JENKINS, D., KLOSE, F., KNAPP, B., LATOUR, B., LETTEBOER, S. J., MARCELIS, C. L., MITIC, D., MORLEO, M., OUD, M. M., RIEMERSMA, M., RIX, S., TERHAL, P. A., TOEDT, G., VAN DAM, T. J., DE VRIEZE, E., WISSINGER, Y., WU, K. M., APIC, G., BEALES, P. L., BLACQUE, O. E., GIBSON, T. J., HUYNEN, M. A., KATSANIS, N., KREMER, H., OMRAN, H., VAN WIJK, E., WOLFRUM, U., KEPES, F., DAVIS, E. E., FRANCO, B., GILES, R. H., UEFFING, M., RUSSELL, R. B., ROEPMAN, R. & GROUP, U. K. R. D. 2016. An organelle-specific protein landscape identifies novel diseases and molecular mechanisms. *Nat Commun,* 7**,** 11491.

BRIGIDI, G. S., SANTYR, B., SHIMELL, J., JOVELLAR, B. & BAMJI, S. X. 2015. Activity-regulated trafficking of the palmitoyl-acyl transferase DHHC5. *Nat Commun,* 6**,** 8200.

CAMPEAU, E., RUHL, V. E., RODIER, F., SMITH, C. L., RAHMBERG, B. L., FUSS, J. O., CAMPISI, J., YASWEN, P., COOPER, P. K. & KAUFMAN, P. D. 2009. A versatile viral system for expression and depletion of proteins in mammalian cells. *PLoS One,* 4**,** e6529.

CEVIK, S., HORI, Y., KAPLAN, O. I., KIDA, K., TOIVENON, T., FOLEY-FISHER, C., COTTELL, D., KATADA, T., KONTANI, K. & BLACQUE, O. E. 2010. Joubert syndrome Arl13b functions at ciliary membranes and stabilizes protein transport in Caenorhabditis elegans. *J Cell Biol,* 188**,** 953-69.

CHACON-HESZELE, M. F., CHOI, S. Y., ZUO, X., BAEK, J. I., WARD, C. & LIPSCHUTZ, J. H. 2014. The exocyst and regulatory GTPases in urinary exosomes. *Physiol Rep,* 2.

CLUPPER, M., GILL, R., ELSAYYID, M., TOUROUTINE, D., CAPLAN, J. L. & TANIS, J. E. 2022. Kinesin-2 motors differentially impact biogenesis of extracellular vesicle subpopulations shed from sensory cilia. *iScience,* 25**,** 105262.

DIENER, D. R., LUPETTI, P. & ROSENBAUM, J. L. 2015. Proteomic analysis of isolated ciliary transition zones reveals the presence of ESCRT proteins. *Curr Biol,* 25**,** 379-384.

DIXSON, A. C., DAWSON, T. R., DI VIZIO, D. & WEAVER, A. M. 2023. Context-specific regulation of extracellular vesicle biogenesis and cargo selection. *Nat Rev Mol Cell Biol,* 24**,** 454-476.

DOENCH, J. G., FUSI, N., SULLENDER, M., HEGDE, M., VAIMBERG, E. W., DONOVAN, K. F., SMITH, I., TOTHOVA, Z., WILEN, C., ORCHARD, R., VIRGIN, H. W., LISTGARTEN, J. & ROOT, D. E. 2016. Optimized sgRNA design to maximize activity and minimize off-target effects of CRISPR-Cas9. *Nat Biotechnol,* 34**,** 184-191.

DOYLE, L. M. & WANG, M. Z. 2019. Overview of Extracellular Vesicles, Their Origin, Composition, Purpose, and Methods for Exosome Isolation and Analysis. *Cells,* 8.

DUBREUIL, V., MARZESCO, A. M., CORBEIL, D., HUTTNER, W. B. & WILSCH-BRAUNINGER, M. 2007. Midbody and primary cilium of neural progenitors release extracellular membrane particles enriched in the stem cell marker prominin-1. *J Cell Biol,* 176**,** 483-95.

FOGELGREN, B., LIN, S. Y., ZUO, X., JAFFE, K. M., PARK, K. M., REICHERT, R. J., BELL, P. D., BURDINE, R. D. & LIPSCHUTZ, J. H. 2011. The exocyst protein Sec10 interacts with Polycystin-2 and knockdown causes PKD-phenotypes. *PLoS Genet,* 7**,** e1001361.

FOLLIT, J. A., SAN AGUSTIN, J. T., XU, F., JONASSEN, J. A., SAMTANI, R., LO, C. W. & PAZOUR, G. J. 2008. The Golgin GMAP210/TRIP11 anchors IFT20 to the Golgi complex. *PLoS Genet,* 4**,** e1000315.

FOLLIT, J. A., TUFT, R. A., FOGARTY, K. E. & PAZOUR, G. J. 2006. The intraflagellar transport protein IFT20 is associated with the Golgi complex and is required for cilia assembly. *Mol Biol Cell,* 17**,** 3781-92.

GONCALVES, A. B., HASSELBALCH, S. K., JOENSEN, B. B., PATZKE, S., MARTENS, P., OHLSEN, S. K., QUINODOZ, M., NIKOPOULOS, K., SULEIMAN, R., DAMSO JEPPESEN, M. P., WEISS, C., CHRISTENSEN, S. T., RIVOLTA, C., ANDERSEN, J. S., FARINELLI, P. & PEDERSEN, L. B. 2021. CEP78 functions downstream of CEP350 to control biogenesis of primary cilia by negatively regulating CP110 levels. *Elife,* 10.

HE, K., MA, X., XU, T., LI, Y., HODGE, A., ZHANG, Q., TORLINE, J., HUANG, Y., ZHAO, J., LING, K. & HU, J. 2018. Axoneme polyglutamylation regulated by Joubert syndrome protein ARL13B controls ciliary targeting of signaling molecules. *Nat Commun,* 9**,** 3310.

HOFFMEISTER, H., BABINGER, K., GURSTER, S., CEDZICH, A., MEESE, C., SCHADENDORF, K., OSTEN, L., DE VRIES, U., RASCLE, A. & WITZGALL, R. 2011. Polycystin-2 takes different routes to the somatic and ciliary plasma membrane. *J Cell Biol,* 192**,** 631-45.

HOGAN, M. C., MANGANELLI, L., WOOLLARD, J. R., MASYUK, A. I., MASYUK, T. V., TAMMACHOTE, R., HUANG, B. Q., LEONTOVICH, A. A., BEITO, T. G., MADDEN, B. J., CHARLESWORTH, M. C., TORRES, V. E., LARUSSO, N. F., HARRIS, P. C. & WARD, C. J. 2009. Characterization of PKD protein-positive exosome-like vesicles. *J Am Soc Nephrol,* 20**,** 278-88.

HU, J. & HARRIS, P. C. 2020. Regulation of polycystin expression, maturation and trafficking. *Cell Signal,* 72**,** 109630.

HU, J., WITTEKIND, S. G. & BARR, M. M. 2007. STAM and Hrs down-regulate ciliary TRP receptors. *Molecular biology of the cell,* 18**,** 3277-89.

HUANG, F., SIRINAKIS, G., ALLGEYER, E. S., SCHROEDER, L. K., DUIM, W. C., KROMANN, E. B., PHAN, T., RIVERA-MOLINA, F. E., MYERS, J. R., IRNOV, I., LESSARD, M., ZHANG, Y., HANDEL, M. A., JACOBS-WAGNER, C., LUSK, C. P., ROTHMAN, J. E., TOOMRE, D., BOOTH, M. J. & BEWERSDORF, J. 2016. Ultra-High Resolution 3D Imaging of Whole Cells. *Cell,* 166**,** 1028-1040.

HUGHES, J., WARD, C. J., PERAL, B., ASPINWALL, R., CLARK, K., SAN MILLAN, J. L., GAMBLE, V. & HARRIS, P. C. 1995. The polycystic kidney disease 1 (PKD1) gene encodes a novel protein with multiple cell recognition domains. *Nat Genet,* 10**,** 151-60.

JUHL, A. D., ANVARIAN, Z., KUHNS, S., BERGES, J., ANDERSEN, J. S., WUSTNER, D. & PEDERSEN, L. B. 2023. Transient accumulation and bidirectional movement of KIF13B in primary cilia. *J Cell Sci,* 136.

KANAI, Y., WANG, D. & HIROKAWA, N. 2014. KIF13B enhances the endocytosis of LRP1 by recruiting LRP1 to caveolae. *J Cell Biol,* 204**,** 395-408.

KIESEL, P., ALVAREZ VIAR, G., TSOY, N., MARASPINI, R., GORILAK, P., VARGA, V., HONIGMANN, A. & PIGINO, G. 2020. The molecular structure of mammalian primary cilia revealed by cryo-electron tomography. *Nat Struct Mol Biol,* 27**,** 1115-1124.

LAMASON, R. L., KUPFER, A. & POMERANTZ, J. L. 2010. The dynamic distribution of CARD11 at the immunological synapse is regulated by the inhibitory kinesin GAKIN. *Mol Cell,* 40**,** 798-809.

LI, Y., WEI, Q., ZHANG, Y., LING, K. & HU, J. 2010. The small GTPases ARL-13 and ARL-3 coordinate intraflagellar transport and ciliogenesis. *J Cell Biol,* 189**,** 1039-51.

LONG, H., ZHANG, F., XU, N., LIU, G., DIENER, D. R., ROSENBAUM, J. L. & HUANG, K. 2016. Comparative Analysis of Ciliary Membranes and Ectosomes. *Curr Biol,* 26**,** 3327-3335.

LUO, L., ROY, S., LI, L. & MA, M. 2023. Polycystic kidney disease: novel insights into polycystin function. *Trends Mol Med,* 29**,** 268-281.

MA, M., GALLAGHER, A. R. & SOMLO, S. 2017. Ciliary Mechanisms of Cyst Formation in Polycystic Kidney Disease. *Cold Spring Harb Perspect Biol,* 9.

MAGNIFICO, A., ETTENBERG, S., YANG, C., MARIANO, J., TIWARI, S., FANG, S., LIPKOWITZ, S. & WEISSMAN, A. M. 2003. WW domain HECT E3s target Cbl RING finger E3s for proteasomal degradation. *J Biol Chem,* 278**,** 43169-77.

MILL, P., CHRISTENSEN, S. T. & PEDERSEN, L. B. 2023. Primary cilia as dynamic and diverse signalling hubs in development and disease. *Nat Rev Genet,* 24**,** 421-441.

MOCHIZUKI, T., WU, G., HAYASHI, T., XENOPHONTOS, S. L., VELDHUISEN, B., SARIS, J. J., REYNOLDS, D. M., CAI, Y., GABOW, P. A., PIERIDES, A., KIMBERLING, W. J., BREUNING, M. H., DELTAS, C. C., PETERS, D. J. & SOMLO, S. 1996. PKD2, a Gene for Polycystic Kidney Disease That Encodes an Integral Membrane Protein. *Science,* 272**,** 1339-42.

MONIS, W. J., FAUNDEZ, V. & PAZOUR, G. J. 2017. BLOC-1 is required for selective membrane protein trafficking from endosomes to primary cilia. *J Cell Biol,* 216**,** 2131-2150.

MONTESANO, R., GHZILI, H., CARROZZINO, F., ROSSIER, B. C. & FERAILLE, E. 2009. cAMP-dependent chloride secretion mediates tubule enlargement and cyst formation by cultured mammalian collecting duct cells. *Am J Physiol Renal Physiol,* 296**,** F446-57.

MORTHORST, S. K., NIELSEN, C., FARINELLI, P., ANVARIAN, Z., RASMUSSEN, C. B. R., SERRA-MARQUES, A., GRIGORIEV, I., ALTELAAR, M., FURSTENBERG, N., LUDWIG, A., AKHMANOVA, A., CHRISTENSEN, S. T. & PEDERSEN, L. B. 2022. Angiomotin isoform 2 promotes binding of PALS1 to KIF13B at primary cilia and regulates ciliary length and signaling. *J Cell Sci,* 135.

NACHURY, M. V., LOKTEV, A. V., ZHANG, Q., WESTLAKE, C. J., PERANEN, J., MERDES, A., SLUSARSKI, D. C., SCHELLER, R. H., BAZAN, J. F., SHEFFIELD, V. C. & JACKSON, P. K. 2007. A core complex of BBS proteins cooperates with the GTPase Rab8 to promote ciliary membrane biogenesis. *Cell,* 129**,** 1201-13.

NACHURY, M. V. & MICK, D. U. 2019. Establishing and regulating the composition of cilia for signal transduction. *Nat Rev Mol Cell Biol,* 20**,** 389-405.

NAGER, A. R., GOLDSTEIN, J. S., HERRANZ-PEREZ, V., PORTRAN, D., YE, F., GARCIA-VERDUGO, J. M. & NACHURY, M. V. 2017. An Actin Network Dispatches Ciliary GPCRs into Extracellular Vesicles to Modulate Signaling. *Cell,* 168**,** 252-263

NGUYEN, T. D., TRUONG, M. E. & REITER, J. F. 2022. The Intimate Connection Between Lipids and Hedgehog Signaling. *Front Cell Dev Biol,* 10**,** 876815.

NIKONOROVA, I. A., WANG, J., COPE, A. L., TILTON, P. E., POWER, K. M., WALSH, J. D., AKELLA, J. S., KRAUCHUNAS, A. R., SHAH, P. & BARR, M. M. 2022. Isolation, profiling, and tracking of extracellular vesicle cargo in Caenorhabditis elegans. *Curr Biol,* 32**,** 1924-1936 e6.

O'CONNOR, H. F., LYON, N., LEUNG, J. W., AGARWAL, P., SWAIM, C. D., MILLER, K. M. & HUIBREGTSE, J. M. 2015. Ubiquitin-Activated Interaction Traps (UBAITs) identify E3 ligase binding partners. *EMBO Rep,* 16**,** 1699-712.

OJEDA NAHARROS, I. & NACHURY, M. V. 2022. Shedding of ciliary vesicles at a glance. *J Cell Sci,* 135.

PAZOUR, G. J., SAN AGUSTIN, J. T., FOLLIT, J. A., ROSENBAUM, J. L. & WITMAN, G. B. 2002. Polycystin-2 localizes to kidney cilia and the ciliary level is elevated in orpk mice with polycystic kidney disease. *Curr Biol,* 12**,** R378-80.

PEDEN, E. M. & BARR, M. M. 2005. The KLP-6 kinesin is required for male mating behaviors and polycystin localization in *Caenorhabditis elegans*. *Curr Biol,* 15**,** 394-404.

RAN, F. A., HSU, P. D., WRIGHT, J., AGARWALA, V., SCOTT, D. A. & ZHANG, F. 2013. Genome engineering using the CRISPR-Cas9 system. *Nat Protoc,* 8**,** 2281-2308.

REITER, J. F. & LEROUX, M. R. 2017. Genes and molecular pathways underpinning ciliopathies. *Nat Rev Mol Cell Biol,* 18**,** 533-547.

REZI, C. K., ASLANYAN, M. G., DIWAN, G. D., CHENG, T., CHAMLALI, M., JUNGER, K., ANVARIAN, Z., LORENTZEN, E., PAULY, K. B., AFSHAR-BAHADORI, Y., FERNANDES, E. F. A., QIAN, F., TOSI, S., CHRISTENSEN, S. T., PEDERSEN, S. F., STROMGAARD, K., RUSSELL, R. B., MINER, J. H., MAHJOUB, M. R., BOLDT, K., ROEPMAN, R. & PEDERSEN, L. B. 2023. DLG1 functions upstream of SDCCAG3 and IFT20 to control ciliary targeting of polycystin-2. *bioRxiv*.

ROY, K., JERMAN, S., JOZSEF, L., MCNAMARA, T., ONYEKABA, G., SUN, Z. & MARIN, E. P. 2017. Palmitoylation of the ciliary GTPase ARL13b is necessary for its stability and its role in cilia formation. *J Biol Chem,* 292**,** 17703-17717.

ROY, K. & MARIN, E. P. 2019. Lipid Modifications in Cilia Biology. *J Clin Med,* 8.

SAMSONOV, R., SHTAM, T., BURDAKOV, V., GLOTOV, A., TSYRLINA, E., BERSTEIN, L., NOSOV, A., EVTUSHENKO, V., FILATOV, M. & MALEK, A. 2016. Lectin-induced agglutination method of urinary exosomes isolation followed by mi-RNA analysis: Application for prostate cancer diagnostic. *Prostate,* 76**,** 68-79.

SCHEIDEL, N., KENNEDY, J. & BLACQUE, O. E. 2018. Endosome maturation factors Rabenosyn-5/VPS45 and caveolin-1 regulate ciliary membrane and polycystin-2 homeostasis. *EMBO J,* 37.

SCHOU, K. B., MOGENSEN, J. B., NIELSEN, B. S., MORTHORST, S. K., ALELIUNAITE, A., SERRA-MARQUES, A. M. A., SAUNIER, S., BIZET, A., VELAND, I. R., AKHMANOVA, A., CHRISTENSEN, S. T. & PEDERSEN, L. B. 2017. KIF13B establishes a CAV1-enriched microdomain at the ciliary transition zone to promote Sonic hedgehog signaling. *Nature Communications,* 8**,** 14177.

STRACK, B., CALISTRI, A., CRAIG, S., POPOVA, E. & GOTTLINGER, H. G. 2003. AIP1/ALIX is a binding partner for HIV-1 p6 and EIAV p9 functioning in virus budding. *Cell,* 114**,** 689-99.

SUN, S., FISHER, R. L., BOWSER, S. S., PENTECOST, B. T. & SUI, H. 2019. Three-dimensional architecture of epithelial primary cilia. *Proc Natl Acad Sci U S A,* 116**,** 9370-9379.

TANAKA, Y., MOROZUMI, A. & HIROKAWA, N. 2023. Nodal flow transfers polycystin to determine mouse left-right asymmetry. *Dev Cell,* 58**,** 1447-1461 e6.

TIAN, H., LU, J. Y., SHAO, C., HUFFMAN, K. E., CARSTENS, R. M., LARSEN, J. E., GIRARD, L., LIU, H., RODRIGUEZ-CANALES, J., FRENKEL, E. P., WISTUBA, II, MINNA, J. D. & HOFMANN, S. L. 2015. Systematic siRNA Screen Unmasks NSCLC Growth Dependence by Palmitoyltransferase DHHC5. *Mol Cancer Res,* 13**,** 784-94.

TRAJKOVIC, K., HSU, C., CHIANTIA, S., RAJENDRAN, L., WENZEL, D., WIELAND, F., SCHWILLE, P., BRUGGER, B. & SIMONS, M. 2008. Ceramide triggers budding of exosome vesicles into multivesicular endosomes. *Science,* 319**,** 1244-7.

VOLZ, A. K., FREI, A., KRETSCHMER, V., DE JESUS DOMINGUES, A. M., KETTING, R. F., UEFFING, M., BOLDT, K., KRAMER-ALBERS, E. M. & MAY-SIMERA, H. L. 2021. Bardet-Biedl syndrome proteins modulate the release of bioactive extracellular vesicles. *Nat Commun,* 12**,** 5671.

VON SCHWEDLER, U. K., STUCHELL, M., MULLER, B., WARD, D. M., CHUNG, H. Y., MORITA, E., WANG, H. E., DAVIS, T., HE, G. P., CIMBORA, D. M., SCOTT, A., KRAUSSLICH, H. G., KAPLAN, J., MORHAM, S. G. & SUNDQUIST, W. I. 2003. The protein network of HIV budding. *Cell,* 114**,** 701-13.

WALKER, R. V., KEYNTON, J. L., GRIMES, D. T., SREEKUMAR, V., WILLIAMS, D. J., ESAPA, C., WU, D., KNIGHT, M. M. & NORRIS, D. P. 2019. Ciliary exclusion of Polycystin-2 promotes kidney cystogenesis in an autosomal dominant polycystic kidney disease model. *Nat Commun,* 10**,** 4072.

WALSH, R. B., DRESSELHAUS, E. C., BECALSKA, A. N., ZUNITCH, M. J., BLANCHETTE, C. R., SCALERA, A. L., LEMOS, T., LEE, S. M., APIKI, J., WANG, S., ISAAC, B., YEH, A., KOLES, K. & RODAL, A. A. 2021. Opposing functions for retromer and Rab11 in extracellular vesicle traffic at presynaptic terminals. *J Cell Biol,* 220.

WANG, J., NIKONOROVA, I. A., SILVA, M., WALSH, J. D., TILTON, P. E., GU, A., AKELLA, J. S. & BARR, M. M. 2021. Sensory cilia act as a specialized venue for regulated extracellular vesicle biogenesis and signaling. *Curr Biol,* 31**,** 3943-3951 e3.

WANG, J., SAUL, J., NIKONOROVA, I. A., CRUZ, C. N., POWER, K. M., NGUYEN, K. C., HALL, D. H. & BARR, M. M. 2023a. Ciliary intrinsic mechanisms regulate dynamic ciliary extracellular vesicle release from sensory neurons. *bioRxiv*.

WANG, J., SILVA, M., HAAS, L. A., MORSCI, N. S., NGUYEN, K. C., HALL, D. H. & BARR, M. M. 2014. C. elegans ciliated sensory neurons release extracellular vesicles that function in animal communication. *Curr Biol,* 24**,** 519-25.

WANG, L., WEN, X., WANG, Z., LIN, Z., LI, C., ZHOU, H., YU, H., LI, Y., CHENG, Y., CHEN, Y., LOU, G., PAN, J. & CAO, M. 2022. Ciliary transition zone proteins coordinate ciliary protein composition and ectosome shedding. *Nat Commun,* 13**,** 3997.

WANG, Y., ZHANG, S., HE, H., LUO, H., XIA, Y., JIANG, Y., JIANG, J. & SUN, L. 2023b. Repositioning Lomitapide to block ZDHHC5-dependant palmitoylation on SSTR5 leads to anti-proliferation effect in preclinical pancreatic cancer models. *Cell Death Discov,* 9**,** 60.

WICKHAM, H. 2016. *ggplot2: Elegant Graphics for Data Analysis (3e),* Springer.

WOOD, C. R., HUANG, K., DIENER, D. R. & ROSENBAUM, J. L. 2013. The cilium secretes bioactive ectosomes. *Curr Biol,* 23**,** 906-11.

WOOD, C. R. & ROSENBAUM, J. L. 2015. Ciliary ectosomes: transmissions from the cell's antenna. *Trends Cell Biol,* 25**,** 276-85.

WRIGHT, M. H., BERLIN, I. & NASH, P. D. 2011. Regulation of endocytic sorting by ESCRT-DUB-mediated deubiquitination. *Cell Biochem Biophys,* 60**,** 39-46.

WU, H., REUVER, S. M., KUHLENDAHL, S., CHUNG, W. J. & GARNER, C. C. 1998. Subcellular targeting and cytoskeletal attachment of SAP97 to the epithelial lateral membrane. *J Cell Biol,* 111**,** 2365-76.

YODER, B. K., HOU, X. & GUAY-WOODFORD, L. M. 2002. The polycystic kidney disease proteins, polycystin-1, polycystin-2, polaris, and cystin, are co-localized in renal cilia. *J Am Soc Nephrol,* 13**,** 2508-16.

YU, F., SHARMA, S., SKOWRONEK, A. & ERDMANN, K. S. 2016. The serologically defined colon cancer antigen-3 (SDCCAG3) is involved in the regulation of ciliogenesis. *Sci Rep,* 6**,** 35399.

ZHAO, H., KHAN, Z. & WESTLAKE, C. J. 2023. Ciliogenesis membrane dynamics and organization. *Semin Cell Dev Biol,* 133**,** 20-31.

ZHU, J., SHANG, Y., XIA, Y., ZHANG, R. & ZHANG, M. 2016. An Atypical MAGUK GK Target Recognition Mode Revealed by the Interaction between DLG and KIF13B. *Structure,* 24**,** 1876-1885.

Figure 1

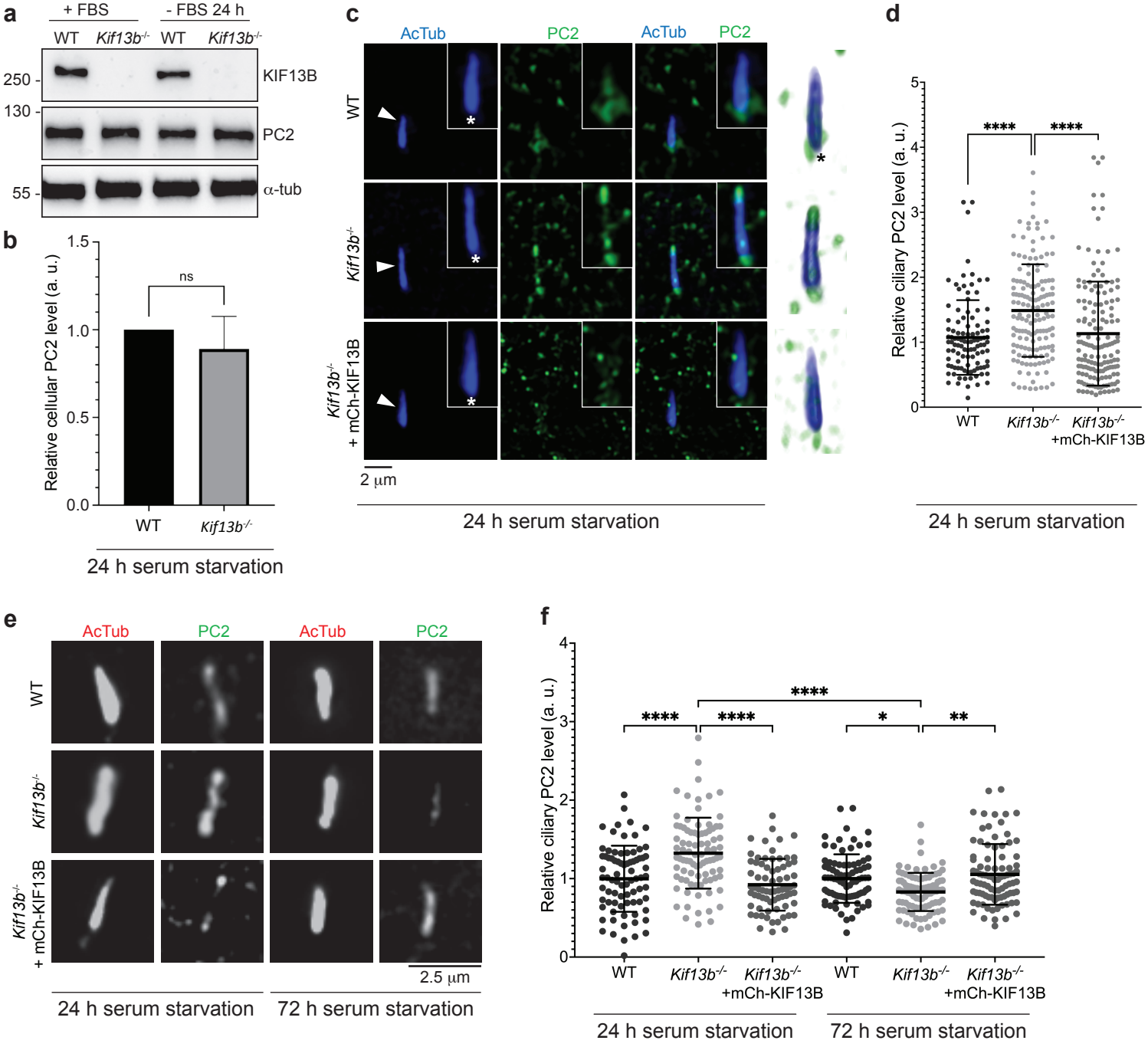
a
+ FBS
- FBS 24 h
WT
Kif13b-/-
WT
Kif13b-/-
250
130
55
KIF13B
PC2
α-tub
b
Relative cellular PC2 level (a. u.)
1.5
1.0
0.5
0.0
ns
WT
Kif13b-/-
24 h serum starvation
c
AcTub
PC2
AcTub
PC2
WT
Kif13b-/-
Kif13b-/- + mCh-KIF13B
2 µm
24 h serum starvation
d
Relative ciliary PC2 level (a. u.)
5
4
3
2
1
0
****
****
WT
Kif13b-/-
Kif13b-/- +mCh-KIF13B
24 h serum starvation
e
AcTub
PC2
AcTub
PC2
WT
Kif13b-/-
Kif13b-/- + mCh-KIF13B
2.5 µm
24 h serum starvation
72 h serum starvation
f
Relative ciliary PC2 level (a. u.)
4
3
2
1
0
****
****
****
*
**
WT
Kif13b-/-
Kif13b-/- +mCh-KIF13B
WT
Kif13b-/-
Kif13b-/- +mCh-KIF13B
24 h serum starvation
72 h serum starvation

Figure 2

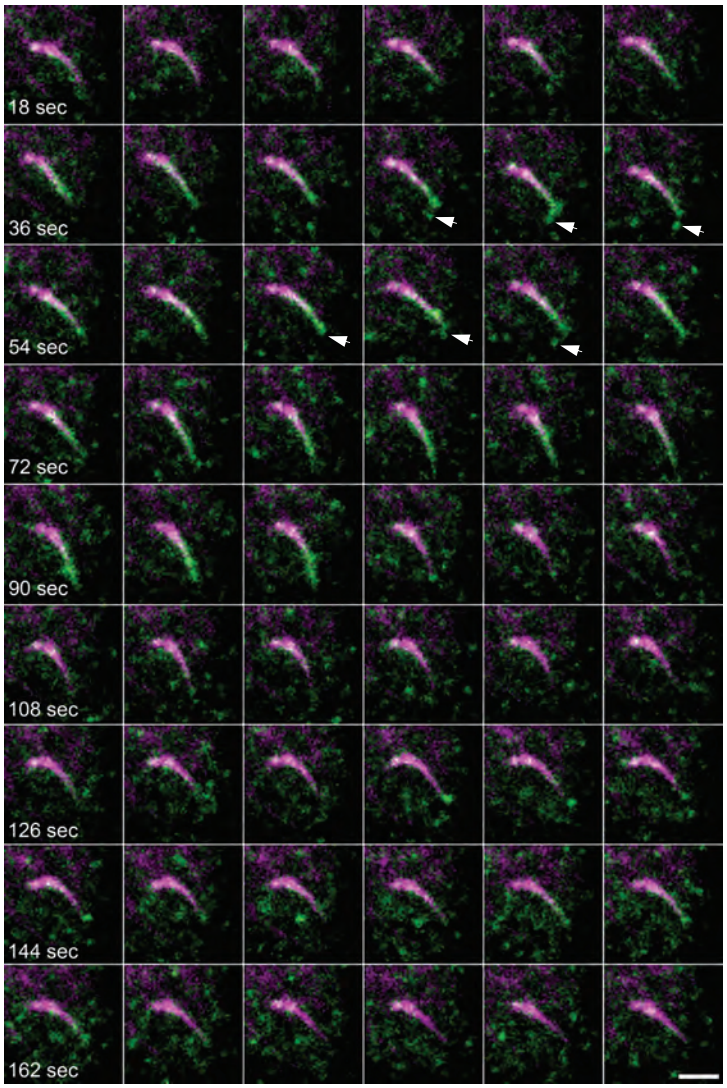

Figure 3

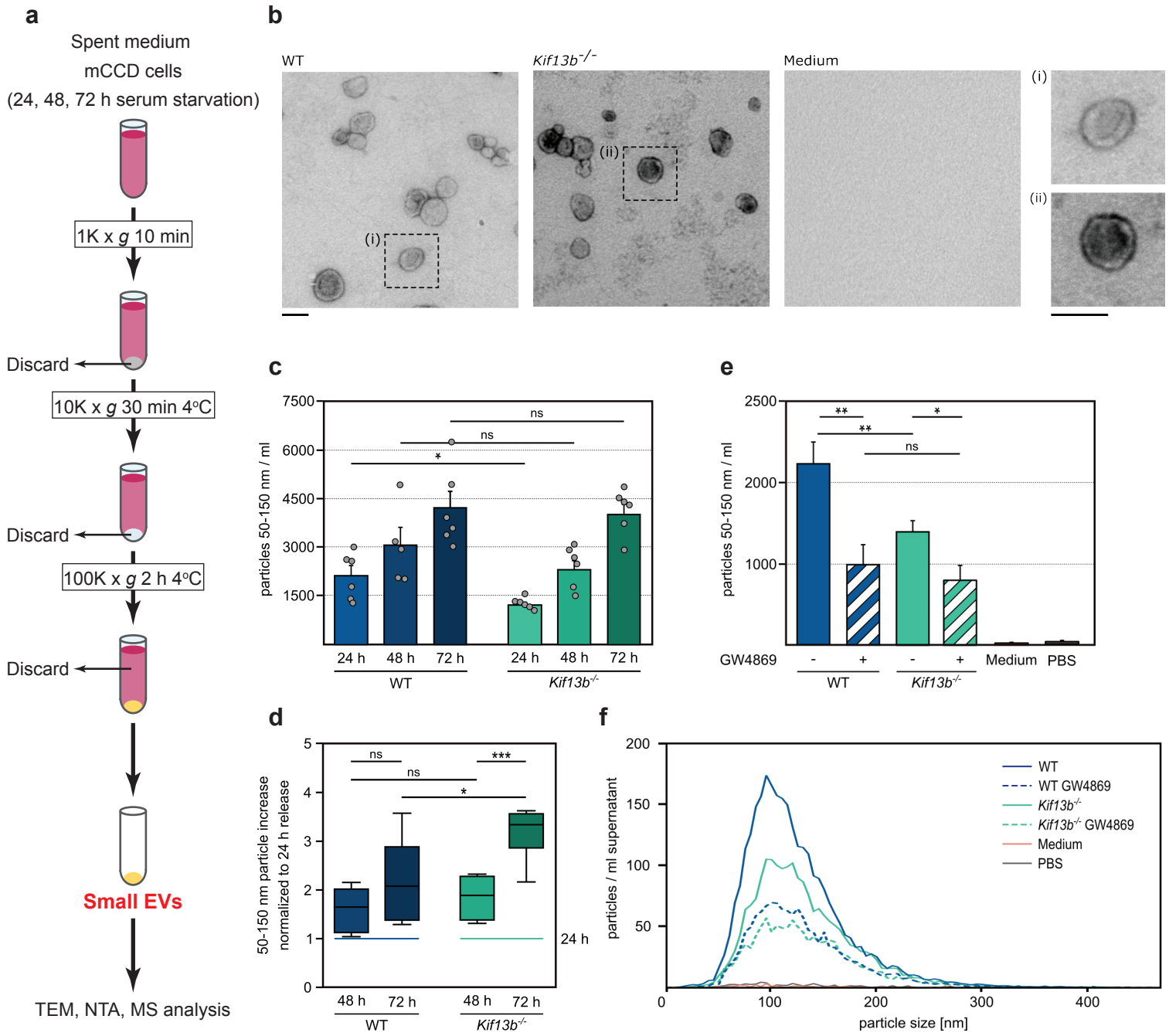
a
Spent medium
mCCD cells
(24, 48, 72 h serum starvation)
1K x g 10 min
Discard
10K x g 30 min 4°C
Discard
100K x g 2 h 4°C
Discard
Small EVs
TEM, NTA, MS analysis
b
WT
Kif13b-/-
Medium
(i)
(ii)
c
particles 50-150 nm / ml
24 h
48 h
72 h
WT
Kif13b-/-
ns
*
d
50-150 nm particle increase normalized to 24 h release
48 h
72 h
WT
Kif13b-/-
ns
***
*
24 h
e
particles 50-150 nm / ml
GW4869
Medium
PBS
**
*
ns
f
particles / ml supernatant
particle size [nm]
WT
WT GW4869
Kif13b-/-
Kif13b-/- GW4869
Medium
PBS

Figure 4

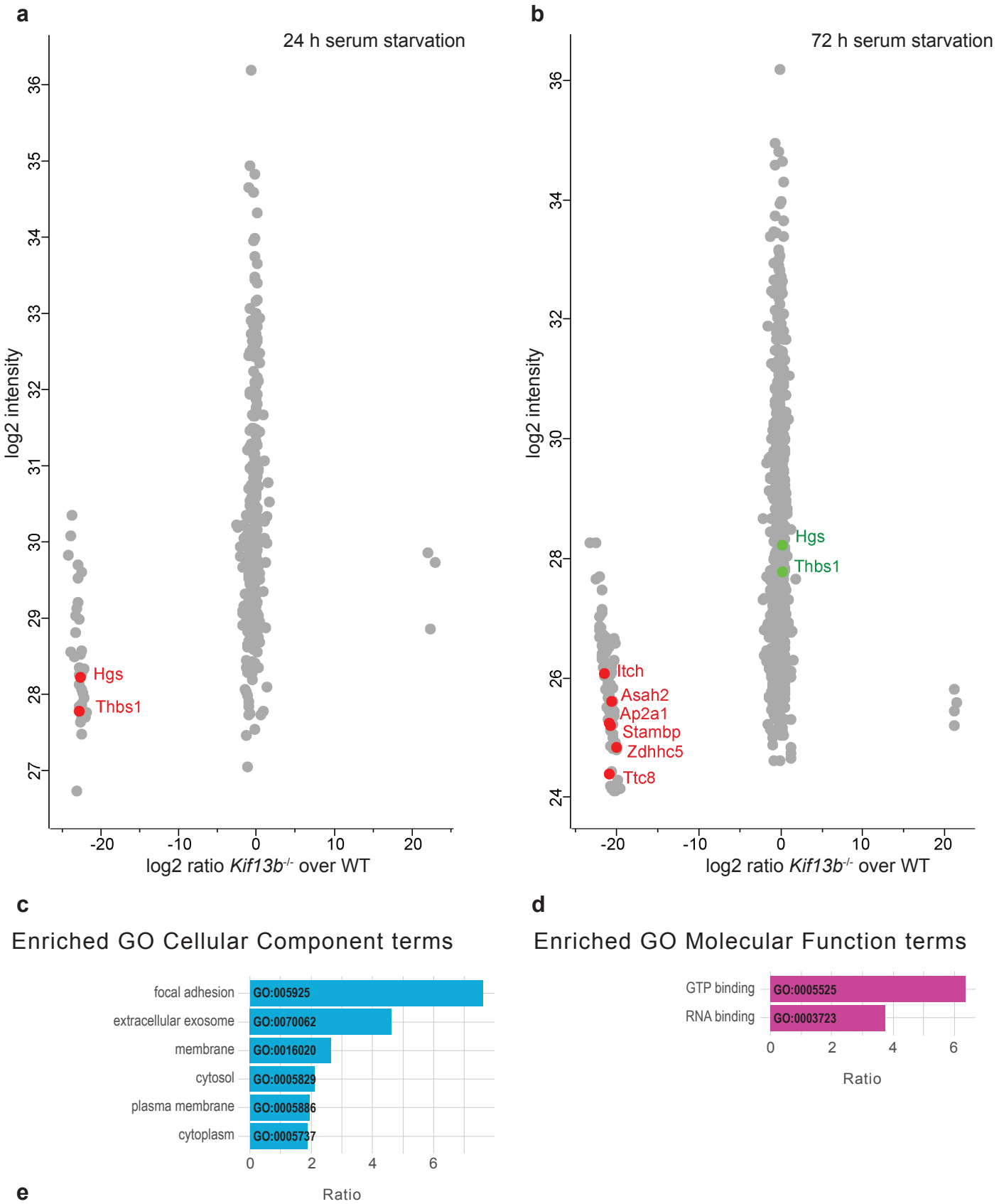

e

Abcg2, Acat2, Acot7, Aga, Aifm1, Ap2a1, Arhgap18, Arl4c, Arpc5, Asah1, **Asah2**, B2m, Ca2, Cdc42ep1, Cdca8, **Cnp**, **Crkl**, Dip2b, Ftl1;Ftl2, Glipr2, Gpd1l, Gpr126, Hnrnpa0, Hnrnpab, Homer3, **Itch**, Itfg3, Mme, Nras, **Ola1,** Pa2g4, **Pdap1**, Pfdn6, Phb2, **Plekhb2**, Rhob, Rpl10a, Rps18, Rtcb, Sec13, Serinc3, Srsf3, Stambp, **Tgm2**, Tmprss2, **Tnpo1**, Top1, Tra2b, Ttc8, **Usp6nl**, **Vamp3;Vamp2**, **Zdhhc5**

Figure 5

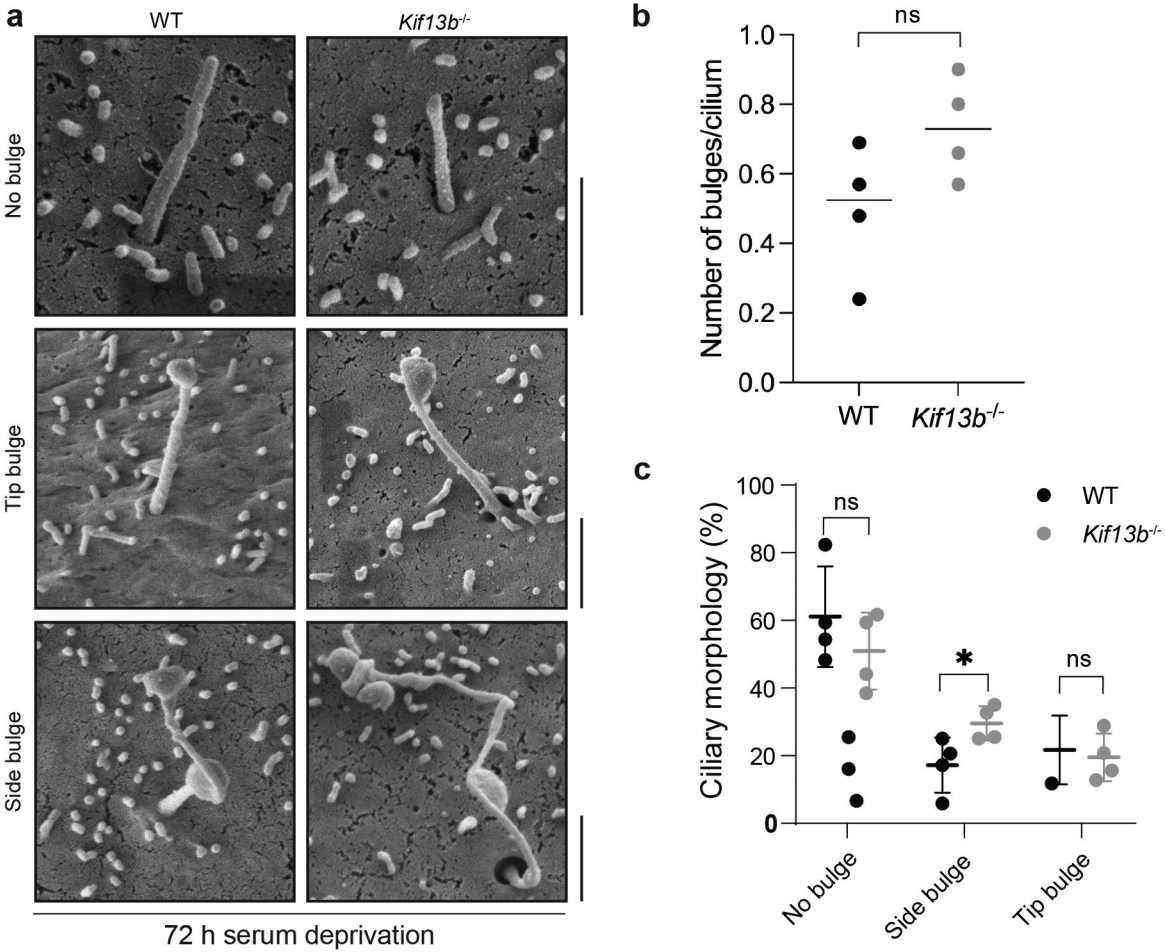
a
WT
Kif13b-/-
No bulge
Tip bulge
Side bulge
72 h serum deprivation
b
ns
Number of bulges/cilium
1.0
0.8
0.6
0.4
0.2
0.0
WT
Kif13b-/-
c
Ciliary morphology (%)
100
80
60
40
20
0
ns
*
ns
WT
Kif13b-/-
No bulge
Side bulge
Tip bulge

Figure 6

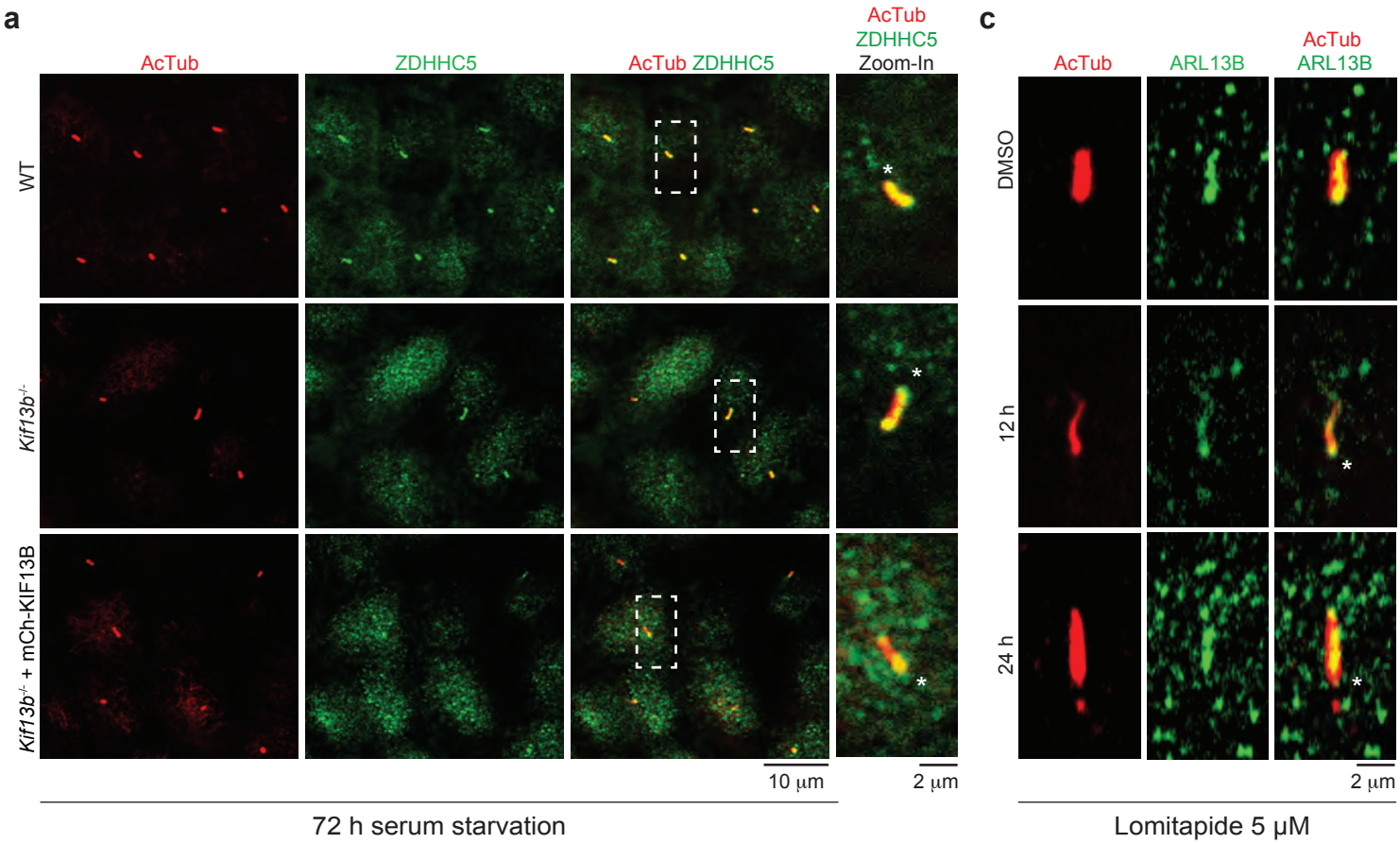
a
AcTub
ZDHHC5
AcTub ZDHHC5
AcTub ZDHHC5 Zoom-In
WT
Kif13b-/-
Kif13b-/- + mCh-KIF13B
10 μm
2 μm
72 h serum starvation
c
AcTub
ARL13B
AcTub ARL13B
DMSO
12 h
24 h
2 μm
Lomitapide 5 μM

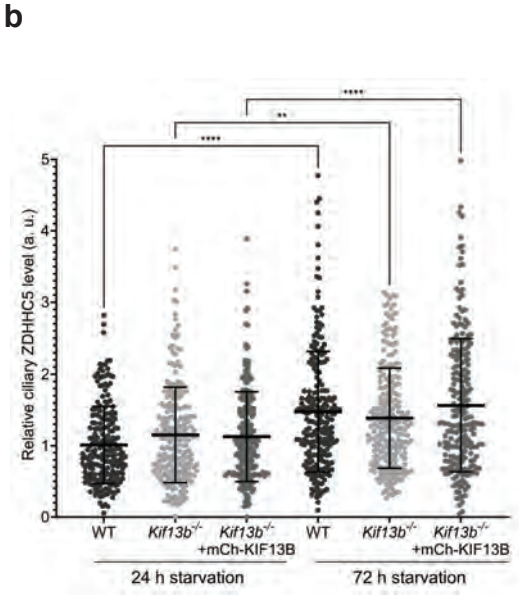
b
Relative ciliary ZDHHC5 level (a. u.)
WT
Kif13b-/-
Kif13b-/- +mCh-KIF13B
24 h starvation
72 h starvation

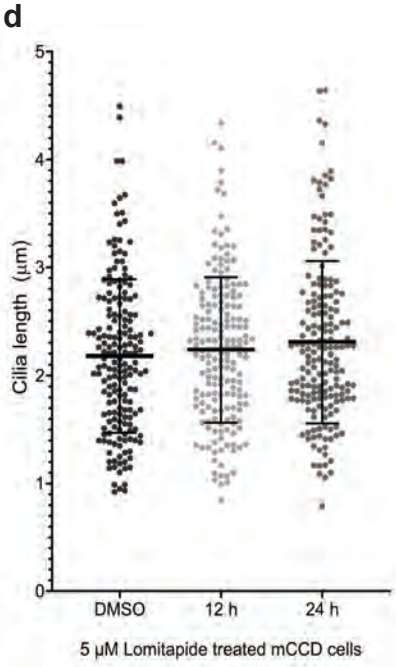
d
Cilia length (μm)
DMSO
12 h
24 h
5 μM Lomitapide treated mCCD cells

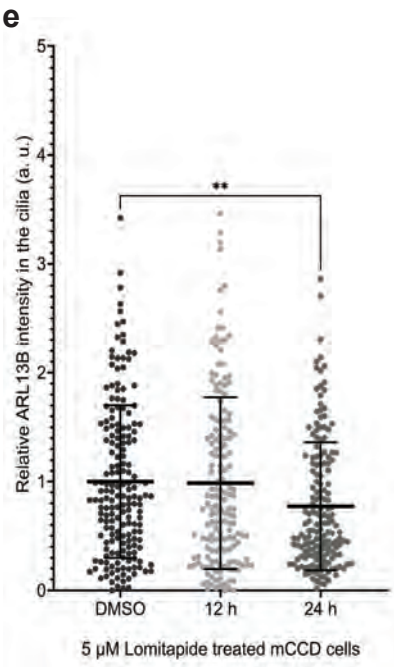
e
Relative ARL13B intensity in the cilia (a. u.)
DMSO
12 h
24 h
5 μM Lomitapide treated mCCD cells

Figure 7

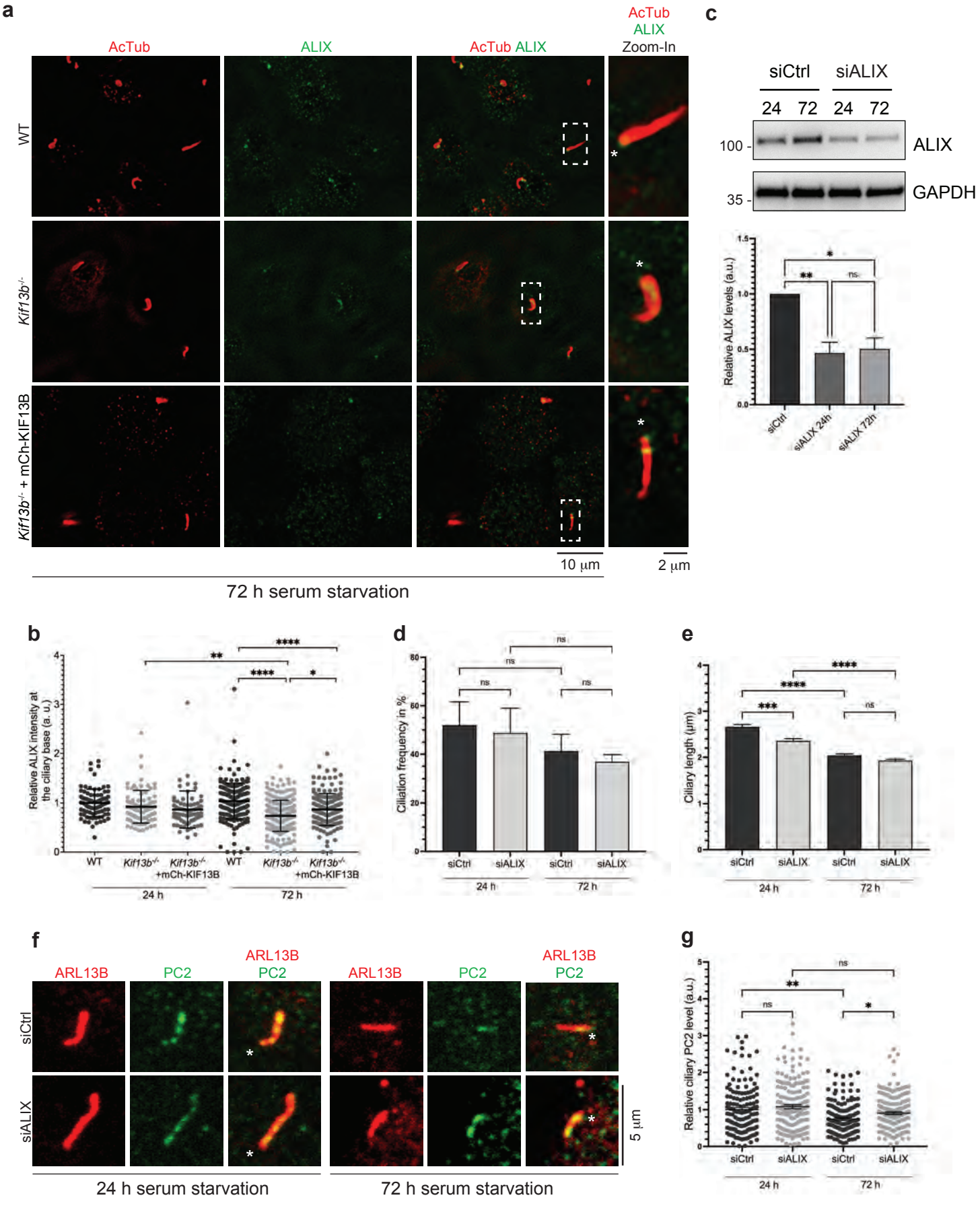
a
AcTub
ALIX
AcTub ALIX
AcTub
ALIX
Zoom-In
WT
Kif13b-/-
Kif13b-/- + mCh-KIF13B
10 µm
2 µm
72 h serum starvation
c
siCtrl
siALIX
24
72
24
72
100 -
ALIX
35 -
GAPDH
Relative ALIX levels (a.u.)
siCtrl
siALIX 24h
siALIX 72h
b
Relative ALIX intensity at the ciliary base (a. u.)
WT
Kif13b-/-
Kif13b-/- +mCh-KIF13B
24 h
72 h
d
Ciliation frequency in %
siCtrl
siALIX
24 h
72 h
e
Ciliary length (µm)
siCtrl
siALIX
24 h
72 h
f
ARL13B
PC2
ARL13B PC2
siCtrl
siALIX
5 µm
24 h serum starvation
72 h serum starvation
g
Relative ciliary PC2 level (a.u.)
siCtrl
siALIX
24 h
72 h

Figure 8

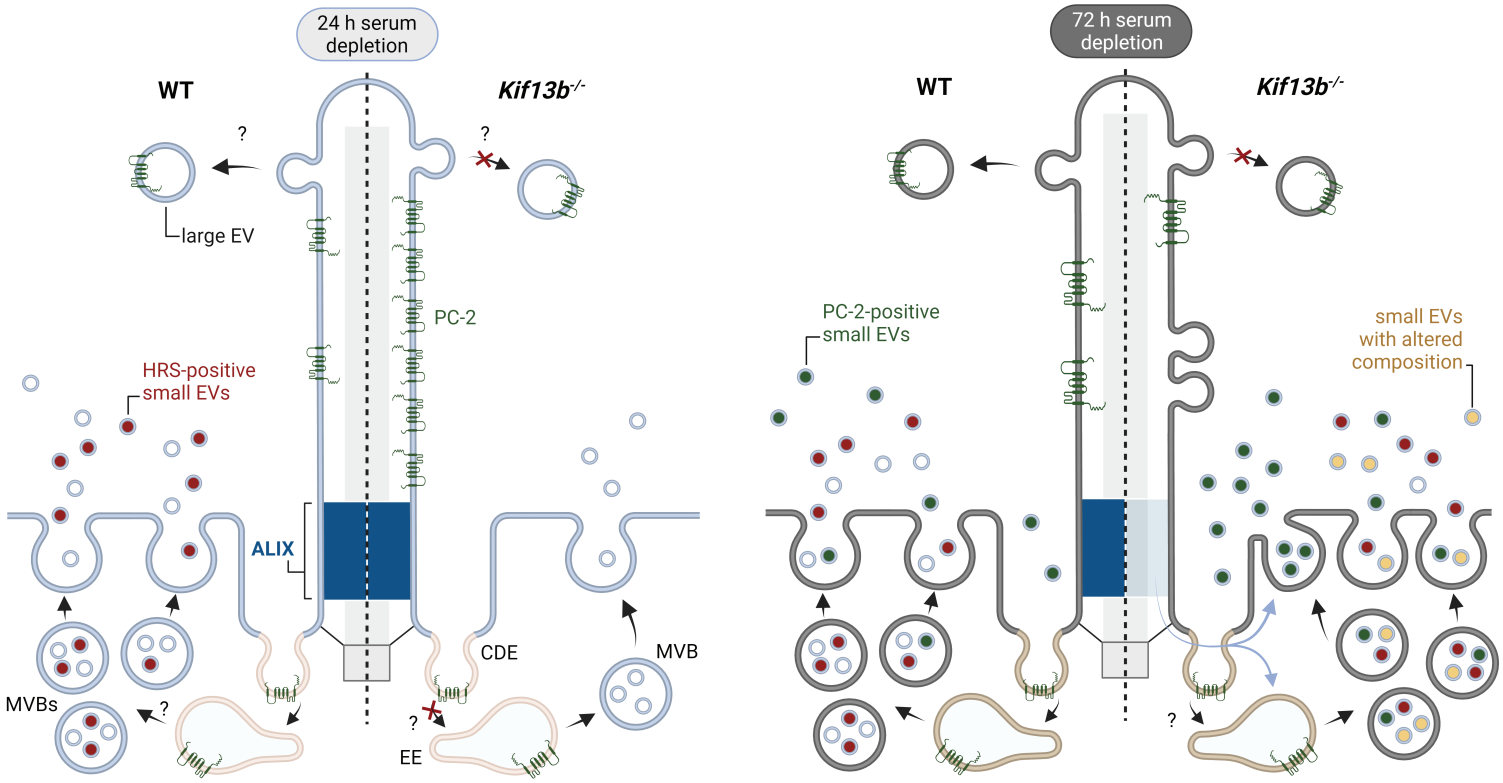
24 h serum depletion
WT
Kif13b-/-
?
?
large EV
PC-2
HRS-positive small EVs
ALIX
CDE
MVB
MVBs
?
?
EE
72 h serum depletion
WT
Kif13b-/-
PC-2-positive small EVs
small EVs with altered composition
?